Ballistic Impact Simulations Using Unified Mechanics Theory

Rimjhim Kashyap

Department of Civil, Structural & Environmental Engineering,

University at Buffalo

Abstract

Ballistic Impact is a high velocity impact on a target by a projectile having a small mass and size. The aim of this paper is to study ballistic impact using the new Unified Mechanics Theory. Numerical simulation of ballistic impact is gaining momentum due to the complexities and large costs involved with experimental study of ballistic impact. But it is seen that most numerical simulations use empirical failure criterion which are based on the results of experiments. The Unified Mechanics Theory however is not based on experimental data curve fitting and does not use any curve fitting techniques to calculate the damage evolution. Entropy production rate alone is used as a metric for damage evolution for elastic and inelastic deformations. This theory can be used for any type of material and for a wide range of damage problems. In this study, an A36 Steel plate has been impacted with a projectile based on a .357 magnum bullet. Finite Element software package ABAQUS/CAE Explicit has been used to numerically simulate the scenario. Analyses have been performed for four different plate temperatures and three different projectile velocities. Damage Evolution Parameter have been calculated using the Unified Mechanics Theory and the results are compared for the different cases to observe trends of variation of the damage initiation time with the temperature of the target and velocity of the projectile.

Introduction

1.1 Ballistic Impact

Ballistic Impact is the high velocity impact on a target by a projectile having a small mass and size. The damage in such an impact happens within fractions of milliseconds. When the projectile hits the target, impact force is applied within a short period of time and this is called shock loading. This shock loading has relatively greater effect on the target than a lower force applied over a proportionally longer period of time.

The reactions and the mechanisms that the occur during a ballistic impact depends upon thickness, strength, ductility, toughness, temperature, acoustic impedance and density of both the target and the projectile and the velocity of the projectile. The maximum velocity at which the projectile fails to penetrate the target is called the ballistic limit of the target and the projectile. At low impact velocities, dynamic deformation mechanisms within the projectile and the target govern the penetration resistance of the target material. However, as the impact velocity increases into the hypervelocity regime, hydrodynamic effects dominate and the penetration response becomes controlled by only the density of the impacted material and projectile.

The study of ballistic impact is of utmost importance in military and defense. This knowledge is useful in developing body armors and other bulletproof objects used in warfare. However, during the development of bulletproof materials, large scale experiments need to be conducted which are expensive and time consuming. Hence, general solution techniques using numerical simulation of ballistic impact are needed to supplement the high-precision testing, so that the experimental costs can be reduced.

The phenomenon of ballistic impact has been well researched both experimentally and numerically. With the help of powerful computational software packages, like ABAQUS, LS-DYNA, etc. ballistic impact can be easily simulated to substitute the expensive experimental setup. However, it is seen that in the numerical simulations, a fracture criterion has to be defined to simulate the fracture in the target. Most numerical simulations use the Johnson-Cook failure initiation criterion, which is an empirical criterion and it is based on the results of experiments. In a recent study, Kumar, Deep et al. (2017) used Lemaitre's Continuum Damage Mechanics model (1984) to study the damage occurring during a ballistic impact. Unified Mechanics Theory was initially proposed in 1998 and has been verified experimentally and mathematically to study the damage occurring in a system using analytical process which is independent of any empirical function. The Unified Mechanics Theory is the unification of Newtonian mechanics and thermodynamics. The theory is based on a thermodynamic framework of damage mechanics of solids and since it is dependent on the entropy generation of the system, it can be used for any system. In this study, the unified mechanics theory has been applied to a system where ballistic impact occurs.

Figure 1.1 Ballistic Impact of a Bullet on a Target

(*Source: http://scienceifl.com/physics/index.htm*)

1.2 Unified Mechanics Theory

The Unified Mechanics Theory originally proposed by Basaran and Yan (1998) provides a thermodynamic framework for damage mechanics of solids, where entropy production is used as the sole measure of damage evolution in the system. There is no need for empirical parameters to define a phenomenological damage potential surface or a Weibull function to trace damage evolution in solid continuum. The theory is founded on the basic premise that a solid continuum obeys the first and second laws of thermodynamics.

The first law of thermodynamics deals with the conservation of energy and the second law deals with the entropy balance. These laws combined with statistical mechanics is used to derive the damage evolution parameter. The damage evolution parameter is only dependent on the internal entropy generation of the system through the entropy difference. This makes the unified mechanics theory independent of the type of material undergoing damage and the type of loading applied, so it can be used for any system, any material and any type of loading.

1.3 Scope of the Study

For the study of ballistic impact using the unified mechanics, the target is chosen to be an A36 steel plate of dimensions 500 mm x 500 mm and thickness 12 mm. The projectile chosen is modeled on a .357 magnum bullet, which has a diameter of 20 mm. The projectile has a cylindrical body of length 80 mm and a conical nose of altitude 20 mm. Numerical modeling of the system has been done using ABAQUS/Explicit Version 6.14 and analysis has been carried out for different plate temperatures and different projectile velocities. The impact of the projectile has been considered normal to the target. Results obtained for these different cases have then been compared to study the effect of these factors on the stresses and strains developed and the damage during the ballistic impact.

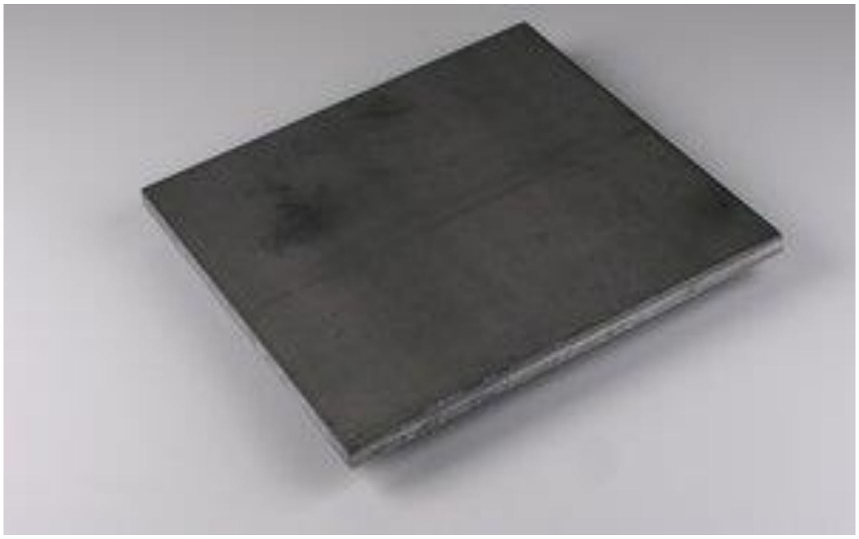

Figure 1.2 A36 Steel Plate (Target)

(*Source:https://www.discountsteel.com/items/A36_Hot_Rolled_Steel_Plate.cfm*)

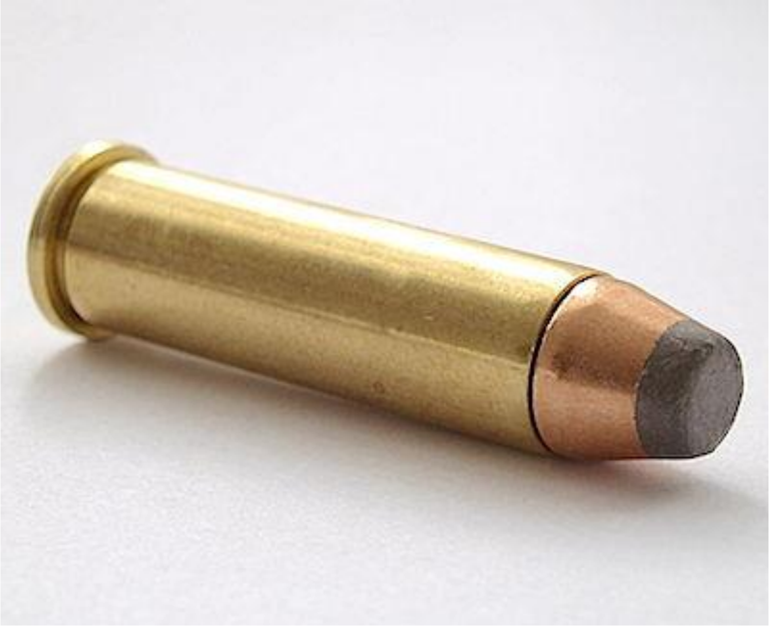

Figure 1.3 .357 Magnum Bullet after which the projectile is modeled

(*Source: https://www.ammoman.com/357-magnum-ammo*)

2.0 Literature Review

2.1 Ballistic Impact

When a ballistic impact occurs, high force is applied over a short period of time, which has a greater effect than force applied over proportionally longer period of time. The damage caused in the target within a small fraction of time due to the collision is highly interesting and has been studied using various phenomenological damage models using Newtonian mechanics.

Anderson Jr and Bodner (1988) states that the simulation of ballistic impacts can be broadly classified into analytical and numerical models. Analytical models are developed from experimental studies, whereas numerical models are developed using computer programs. Ballistic impact has been studied both numerically and experimentally. But due to the complexity and the huge costs involved in studying ballistic impact experimentally, more and more researchers began simulating ballistic impact numerically which is economical and less time consuming. Hydrocodes were used for numerical simulations, which were large computer programs that computed the shock wave interactions. Computational software packages like ABAQUS, LS-DYNA, ANSYS, etc. are now used to numerically simulate and analyze ballistic impact.

Golsdmith and Finnegan (1971) carried out a study of the penetration, perforation and fragmentation of 0.05-0.25 inch thick 2024 aluminum and SAE 1020 and 4130 steel alloy plates impacted normally by 0.125-0.5 inch diameter AISI 52- 100 hard steel spheres at velocities from 500 to 8800 ft/sec. The drop in projectile velocity was found to decrease just above the ballistic limit, then steadily rise with increasing initial bullet speed in all target-projectile configurations. Corran, Shadbolt et al. (1983) conducted a series of experiments on the impact of projectiles at sub-ordnance velocities against mild steel, stainless steel and aluminum plates. It was observed that the projectile mass, nose shape and hardness have an important effect on penetration as does the target rigidity and support condition. Gupta and Madhu (1997) conducted an experimental study of the normal and oblique impact on single and layered plates of mild steel, RHA steel and aluminum of thickness varying from 4.7 mm – 40 mm, by projectiles with impact velocities ranging from 800 m/s – 880 m/s. The experiment also determined the ideal thickness of the plates at ballistic limit.

Børvik, Langseth et al. (2002) conducted a study to study the perforation of 12 mm thick steel plates by 20 mm diameter projectiles with flat, hemispherical and conical noses. The study was carried out in two parts: experimental and numerical. In the experimental phase, gas gun experiments have been used to penetrate 12 mm thick Weldox 460 E steel plate. The impact velocities for the projectiles were around 300 m/s. This experimental study forms basis for explicit finite element analysis using LS-DYNA in the numerical phase. It was found that blunt projectiles caused failure by plugging dominated by shear banding, whereas hemispherical and conical projectiles penetrated the target by mainly pushing the material in front of the projectile aside. The residual velocity was also influenced by the nose shape due to the differences in projectile deformation at impact. Dey, Børvik et al. (2007) studied the effect of target strength on the perforation of three different types of steel plates, Weldox 460 E, Weldox 700 E and Weldox 900 E using three different projectile nose shapes. Compressed gun experiments were carried out to launch projectiles with velocities within 150 m/s – 300 m/s. Later, numerical simulation of these experiments were carried out using LS-DYNA. The test data were used to determine material constants of all three types of steel in a slightly modified version of the Johnson-Cook constitutive equation and fracture criterion (Johnson and Cook 1983). It was seen that for perforation with blunt projectiles the ballistic limit velocity decreases for increasing strength, while the opposite trend is found in tests with conical and ogival projectiles.

Arias, Rodríguez-Martínez et al. (2008) carried out a series numerical simulations of impact behavior of thin steel plates subjected to cylindrical, conical and hemispherical non-deformable projectiles with impact velocities ranging from 190 m/s – 600 m/s using ABAQUS/Explicit. Johnson-Cook model was used to define the thermoviscoplastic behavior of the plate material and Johnson-Cook fracture criterion was used to predict the perforation process. Rusinek, Rodríguez-Martínez et al. (2009) presented an experimental and numerical analysis of the failure process of mild steel sheets subjected to normal impact by hemispherical projectiles. The experimental study was performed using a direct impact technique based on Hopkinson tube as a force measurement device and covered a wide range of impact velocities. The numerical simulations have been done using ABAQUS/Explicit. The material behavior of the specimens was approximated by three different constitutive relations: Johnson–Cook (JC), Rusinek–Klepaczko (RK) and a power law of strain hardening (PL).

Park, Yoo et al. (2005) studied the ballistic impact on multilayered steel and aluminum plates using NET2D, a Lagrangian explicit time-integration finite element code for impact analyses, to find the optimal parameter values. Johnson-Cook model has been used to consider the effects of strain rate hardening, strain hardening and thermal softening. Abdel-Wahed, Salem et al. (2010) studied the normal penetration of armor-piercing projectiles with caliber of 7.62 mm at velocities 300 m/s – 600m/s into single and multi-layered steel plates experimentally as well as numerically using Autodayn-2D hydrocode. Jankowiak, Rusinek et al. (2014) studied the ballistic behavior of steel sheet subjected to impact and perforation by considering a shape function to define the pulse loading during perforation and Johnson-Cook hardening model has been used. Fernandez Ambrosini (2014) studied the normal perforation of 12 mm thick steel plates impacted by 20 mm diameter conical shaped projectiles with impact velocities ranging from 200 m/s – 500 m/s using Johnson-Cook hardening model and fracture criterion. Banerjee, Dhar et al. (2017) performed a numerical simulation of ballistic impact of armor steel plate by ogive-nosed projectiles using Atair-HyperWorks FE package. Johnson-Cook material and failure models have been used to simulate the behavior and failure of the material under impact conditions.

Jena and Senthil (2016) studied the effect of tempering time on the ballistic performance of a high strength armor steel. DMR-1700 steel has been subjected to tempering at 300˚C for 2 hours, 24 hours and 48 hours. Ballistic performance of the samples has been evaluated by impacting 7.62 mm and 12.7 mm armor piercing projectiles at 0° angle of impact. Rahman, Abdullah et al. (2016) studied the ballistic limit of high-strength steel and Al7075-T6 multi-layered plates under 7.62 mm armor piercing projectile at velocity range 900 m/s – 950 m/s. Both projectile and target panels used the Johnson-Cook constitutive material model. The ballistic limits of high-strength steel and Al7075-T6 were obtained numerically by fitting the Recht-Ipson model (Recht and Ipson 1963).

Kumar, Deep et al. (2017) worked on the simulation and analysis of ballistic impact on an IS2062: 2006 GR E410W A steel plate of dimension 500 mm x 500 mm and a thickness of 12 mm by a rigid flat head projectile. The fracture initiation criterion for this model has been developed using Lemaitre's Continuum Damage Mechanics model (Lemaitre 1984). The analysis has been done using ABAQUS/Explicit and the damage growth law has been implemented through a user defined material model subroutine (VUMAT).

Other sophisticated constitutive models that can also be used to model the perforation process were proposed by Zerilli and Armstrong (1987), Abed and Voyiadjis (2005), Rusinek, Zaera et al. (2007). Tupek, Rimoli et al. (2013) studied the ballistic impact of extruded corrugated aluminum panels using a peridynamics damage formulation. More information on the history and developments in the study of ballistic impact can be found in the reviews by Backman and Goldsmith (1978), Corbett, Reid et al. (1996) and Ben-Dor, Dubinsky et al. (2005). Zukas, Nicholas et al. (1982) presented an extensive review of experimental techniques and analytical modeling of ballistic perforation.

2.2 Unified Mechanics Theory

Basaran and Yan (1998) first introduced the damage evolution function based on thermodynamics and statistical physics by establishing a relationship between entropy and damage for solids undergoing plastic deformations. Initial theory was not general enough to account for elastic deformations and to relate entropy production with material stiffness degradation. It was later improved by Basaran and Nie (2004).

According to Unified Mechanics Theory for predicting damage in a solid continuum, a thermodynamic framework is needed. Entropy production rate is the sole measure of damage evolution in the system. There is no need for empirical parameters to define a phenomenological damage potential surface or a Weibull function to trace damage evolution in solid continuum. For experimental validation, monotonic tensile tests and fatigue tests were carried out on a particulate composite consisting of a distribution of ATH flakes in a PMMA matrix. The results were compared to the numerical analysis done using ABAQUS/CAE, where the damage criterion was defined using the entropy generation rate.

The Unified Mechanics Theory has been verified extensively in the laboratory. Zhao et al (1999), Basaran and Chandaroy (2000), Basaran and Tang (2002), Basaran, Lin et al. (2003), Gomez and Basaran (2005), Li and Basaran (2009), Yao and Basaran (2013), Basaran and Gunel (2015) and Temfack and Basaran (2015) , Abdulhamid and Basaran (2001), Gomez and Basaran (2006) , Basaran and Nie (2007), Basaran et al (2008), Yao and Basaran (2012), have used the Unified Mechanics Theory in their works to analyze damage due to a wide range of loads on different types of materials.

Sosnovskiy and Sherbakov (2016) were able to prove the Unified Mechanics Theory mathematically.

Unified Mechanics Theory

In the following section a summary is given.

3.1 Laws of Thermodynamics

Thermodynamics is based on four laws which describe the behavior of fundamental physical quantities under various circumstances. For the purpose of this work, only the following two laws, in combination with statistical mechanics have been considered:

- The first law of thermodynamics or the law of conservation of energy, which states that the total energy of an isolated system is constant, that is, energy can be neither created or destroyed, but can be transformed from one form to another.
- The second law of thermodynamics or the entropy law, also known as the Clausius-Duheim inequity, which states that the total entropy of an isolated system can never decrease over time. The total entropy can remain constant in cases where the system is in equilibrium or undergoing a reversible process. In case of irreversible processes, the total entropy of the system always increases.

3.2 Energy Conservation

The law of conservation of energy can be represented numerically as the variation of total energy of a system due to specific internal heat source per unit time, *r* (J/s.kg) and energy flux, $\vec{J}_e$ (J/s.m^2) across the surface area. This can be written as:

$$\frac{d}{dt}\iiint^{V} \rho e \, dV = -\iint^{\Omega} \vec{J}_e \, d\vec{\Omega} + \iiint^{V} \rho r \, dV \tag{1}$$

Where, ρ is the density in kg/m^3

V is the volume in m^3

e is the specific total energy in J/kg

Ω is the surface area in m^2

The negative of the energy flux is due to the fact that the normal to the surface are outwards. Therefore, a negative energy flux is a positive external input of energy to the system. At local scale, equation (1) can be written as:

$$\frac{\partial \rho e}{\partial t} = -div\,\vec{J}_e + \rho r \tag{2}$$

The total energy is the summation of internal energy, potential energy and kinetic energy and it written as:

$$e = u + \psi + \frac{\vec{v}^2}{2} \tag{3}$$

Where, u is the specific internal energy in J/kg

ψ is the specific potential energy in J/kg

$\vec{v}$ is the velocity in m/s

These energies are converted from one form to another and the total energy of the system is conserved. Since the entropy generation is only linked to internal energy, the internal energy evolution has been derived.

The variation of kinetic and potential energies has been derived from the local conservation of momentum as:

$$\rho \frac{d\vec{v}}{dt} = -div\, \sigma + \rho\vec{b} \tag{4}$$

Where, σ is the stress tensor in Pa

$\vec{b}$ is the body force per unit mass in N/kg

Assuming a conservative body force derived from potential energy as:

$$\vec{b} = -\overrightarrow{grad}\, \psi \qquad \frac{d\psi}{dt} = 0 \tag{5}$$

The local conservation of momentum can be defined by the rate of change of kinetic and potential energy, which is given as:

$$\frac{\partial(\psi + \vec{v}^2/_2)}{\partial t} = -div\left\{\rho\left(\psi + \vec{v}^2/_2\right)\vec{v} - \sigma\vec{v}\right\} - \sigma{:}\, D \tag{6}$$

Where, D is the strain rate tensor in s^{-1}

Putting the value of $\left(\psi + \vec{v}^2/_2\right)$ from equation (3) into equation (6), the following equation for energy conservation is obtained:

$$\frac{\partial\rho e}{\partial t} = \frac{\partial\rho u}{\partial t} - div\left\{\rho\left(\psi + \vec{v}^2/_2\right)\vec{v} - \sigma\vec{v}\right\} - \sigma{:}\, D \tag{7}$$

The relation between heat flux, $\vec{J}_q$ (J/s.m^2) and total energy flux, $\vec{J}_e$ (J/s.m^2) is given as:

$$\vec{J}_e = \rho e\vec{v} - \sigma\vec{v} + \vec{J}_q \tag{8}$$

Equating equations (7) and (2), the internal energy evolution is derived as:

$$\frac{\partial\rho u}{\partial t} = -div\left(\rho u\vec{v} + \vec{J}_q\right) + \sigma{:}\, D + \rho r \tag{9}$$

Equation (9) can be re-written to give a simplified equation of internal energy evolution as:

$$\rho \frac{du}{dt} = -div\vec{J}_q + \sigma : D + \rho r \tag{10}$$

3.3 Entropy Balance

The change in total entropy of a system is due to internal entropy source and total entropy flux across the surface area, which is given as:

$$\frac{d}{dt} \iiint^{V} \rho s \, dV = -\iint^{\Omega} \vec{J}_{s,tot} \, d\vec{\Omega} + \iiint^{V} \gamma \, dV \tag{11}$$

Where, s is the specific entropy in J/K.kg

γ is the specific internal entropy production in J/K.s.m^3

$\vec{J}_{s,tot}$ is the total entropy flux in J/K.s.m^2

At local scale, equation (11) can be written as:

$$\frac{\partial \rho s}{\partial t} = -div\vec{J}_{s,tot} + \gamma \tag{12}$$

Again, $\vec{J}_{s,tot}$ can be expressed as:

$$\vec{J}_{s,tot} = \vec{J}_s + \rho s \vec{v} \tag{13}$$

Where, $\vec{J}_s$ is the entropy flux in J/K.s.m^2

Therefore, equation (12) can be simplified and written as:

$$\rho \frac{ds}{dt} = -div\vec{J}_s + \gamma \tag{14}$$

Now, entropy flux is related to heat flux as:

$$\vec{J}_s = \frac{\vec{J}_q}{T} \tag{15}$$

Using equation (15), equation (14) becomes

$$\rho \frac{ds}{dt} = -div\left(\frac{\vec{J}_q}{T}\right) + \gamma \tag{16}$$

Equation (16) can also be written as:

$$\rho \frac{ds}{dt} = \frac{\vec{J}_q}{T^2} \overrightarrow{grad} T - \frac{div \vec{J}_q}{T} + \gamma \tag{17}$$

Now, entropy and internal energy are related by the following relation:

$$Tds = du - d\omega^e \tag{18}$$

Where, T is the temperature in K

ω^e is the recoverable energy in J/kg

Using equation (15), equation (10) can be re-written as:

$$\rho \frac{ds}{dt} = \frac{1}{T}\left(-div\vec{J}_q + \sigma{:}D + \rho r - \frac{d\omega^e}{dt}\right) \tag{19}$$

Both equation (17) and (19) express the total entropy variation and by equating these equations, internal entropy generation can be expressed as:

$$\gamma = \frac{\sigma{:}D}{T} - \frac{\rho}{T}\frac{d\omega^e}{dt} - \frac{\vec{J}_q}{T^2}\overrightarrow{grad} T + \frac{\rho r}{T} \tag{20}$$

Furthermore, heat flux is proportional to the gradient of temperature, that is,

$$\vec{J}_q = -k\overrightarrow{grad} T \tag{21}$$

And, $$D = \frac{d\omega^e}{dt}, \;\; \varepsilon = \varepsilon^e + \varepsilon^p, \;\; \frac{\rho d\omega^e}{dt} = \sigma{:}\dot{\varepsilon}^e \tag{22}$$

Therefore, equation (20) becomes:

$$\gamma = \frac{\sigma{:}D}{T} + \frac{k}{T^2}|\overrightarrow{grad} T|^2 + \frac{\rho r}{T} \tag{23}$$

The second law of thermodynamics or Claussius-Duheim inequity expresses the irreversibility of processes. Also, the damage undergone by a material is irreversible.

Hence,

$$\gamma \geq 0$$

Or,
$$\frac{\sigma : \dot{\varepsilon}^p}{T} + \frac{k}{T^2} |\overrightarrow{gradT}|^2 + \frac{\rho r}{T} \geq 0 \tag{24}$$

The internal entropy generation is positive according to the second law of thermodynamics. The first term is the plastic work and takes into account the effect of mechanical loading. The second term takes into account the effects of thermal loading. The last term represents any other loading undergone by the system.

3.4 Damage Evolution Parameter

The internal entropy generation is then normalized to find a damage evolution parameter. This damage evolution parameter will be equal to 0 at the initial state of life of the target and will be equal to a value of 1 when the projectile hits the target and damage occurs. The damage evolution parameter is determined via statistical mechanics.

Boltzmann (1964) first used statistical mechanics to give a precise meaning to disorder in gas establish a connection between disorder and internal entropy of a system. The internal entropy is expressed as a function of the disorder function W, which is a unitless quantity that represents the probability that the system will exist in the state relative to all the possible states it could be in, as shown:

$$s_i = \frac{R}{m_s} \ln(\beta * W) \tag{25}$$

Where, R is the Boltzmann gas constant in J/K.mol

m_s is the molar mass in kg/mol

s_i is the internal specific entropy in J/K.kg

β is a scale factor for coherence of mathematical and physical aspect of equation (25). Since R, m_s and s_i are positive quantities and the disorder function is a probability, β is used to enforce that the two sides of the equation have the same sign.

Equation (25) can be written as:

$$W = \frac{1}{\beta} exp\left(s_i \frac{m_s}{R}\right) \tag{26}$$

The damage evolution parameter, D is defined as the ratio of the change in disorder parameter with the respect current state disorder parameter, as:

$$D = \frac{W - W_0}{W} = 1 - exp\left((-(s_i - s_{i0})\frac{m_s}{R})\right) \tag{27}$$

Where, s_{i0} is the initial internal entropy of the system in J/K.kg

The damage evolution parameter is dependent on the internal entropy production through the difference as:

$$(s_i - s_{io}) = \Delta s_i = \int_{t_0}^{t} \frac{\gamma}{\rho} dt \tag{28}$$

Therefore, using equation (23) and equation (28), the difference in internal energy can be written as:

$$\Delta s_i = \int_{t_0}^{t} \frac{\sigma : \dot{\varepsilon}^p}{\rho T} dt + \int_{t_0}^{t} \frac{k}{\rho T^2} |\overrightarrow{grad} T|^2 dt + \int_{t_0}^{t} \frac{r}{T} dt \tag{29}$$

Finite Element Modeling and Analysis

4.1 Finite Element Modeling

The problem has been numerically modeled and analyzed using the finite element software package ABAQUS/CAE Explicit. Explicit analysis is used in case of an impact problem because the dynamic force which is applied is very large compared to the time period and involves large deformations and nonlinear material response. This procedure solves every problem as a wave propagation problem. ABAQUS Explicit provides the capability to analyze problems involving high-speed (short duration) dynamics, large, nonlinear, quasi-static analyses, highly discontinuous, post-buckling and collapse simulations. Therefore, ABAQUS Explicit has been used in this case to study the ballistic impact problem for this research.

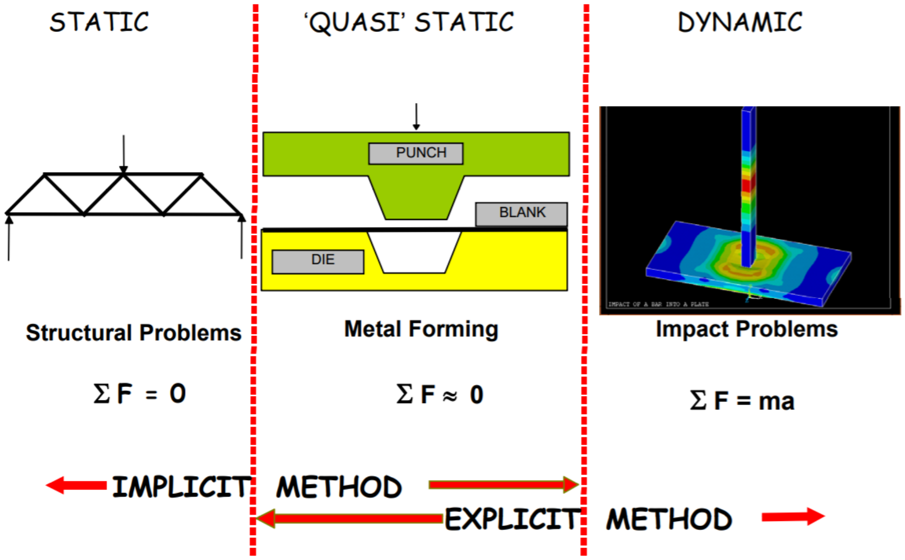

Figure 4.1 Types of problems and the type of method used (*Source:* pdfs.semanticscholar.org/presentation/5c9a/d0e95fbcde98f554a4f69a31ec173f86d4b2.pdf)

4.2 Modeling the target

The target is an A36 Steel plate with dimensions 500 mm x 500 mm and thickness 12 mm. It has been modeled as a 3D deformable solid. A circular partition of diameter 200 mm has been made at the center of the plate. This partition has been meshed finer than the rest of the plate because the projectile will hit at the center of the plate and the stresses and strains will be localized. The material of the plate is A36 Steel. Since the plate is studied at different temperatures, temperature-dependent materials properties have been obtained from relationships given in Eurocode-3 (Standard 2006). These properties and their trends with temperature have been listed in Appendix-A. The Poisson’s ratio and density is assumed to be the same throughout. Milke, Kodur et al. (2002) proposed stress-stress curves for A36 steel at 20˚C, 200˚C, 400˚C and 600˚C and these have been used to define the stress-strain behavior.

The plate has been meshed into a total of 5829 elements of type C3D8RT (an 8-node thermally coupled brick, trilinear displacement and temperature, reduced integration, hourglass control element) and a total number of 11860 nodes. Out of this 1558 elements are in the partition region and has been assigned a seed size of 5 mm to create a finer mesh. The rest of the 4271 elements have been assigned a seed size of 10 mm. The plate is fixed on all sides and the temperature of the plate has been assigned as a pre-defined field.

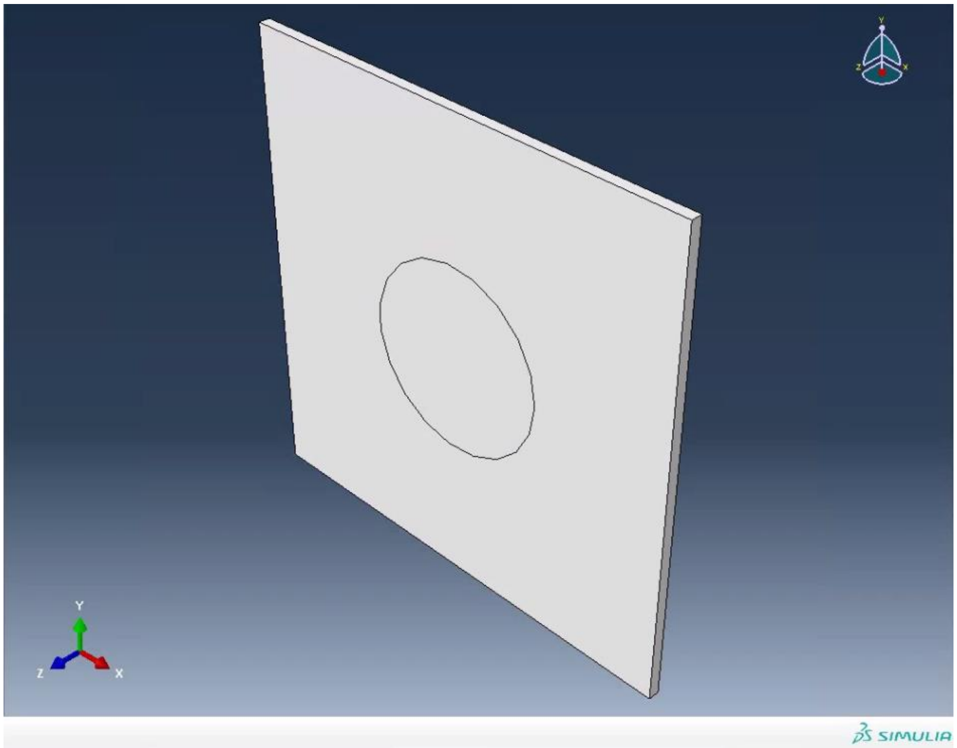

Figure 4.2 3D view of plate part with partition

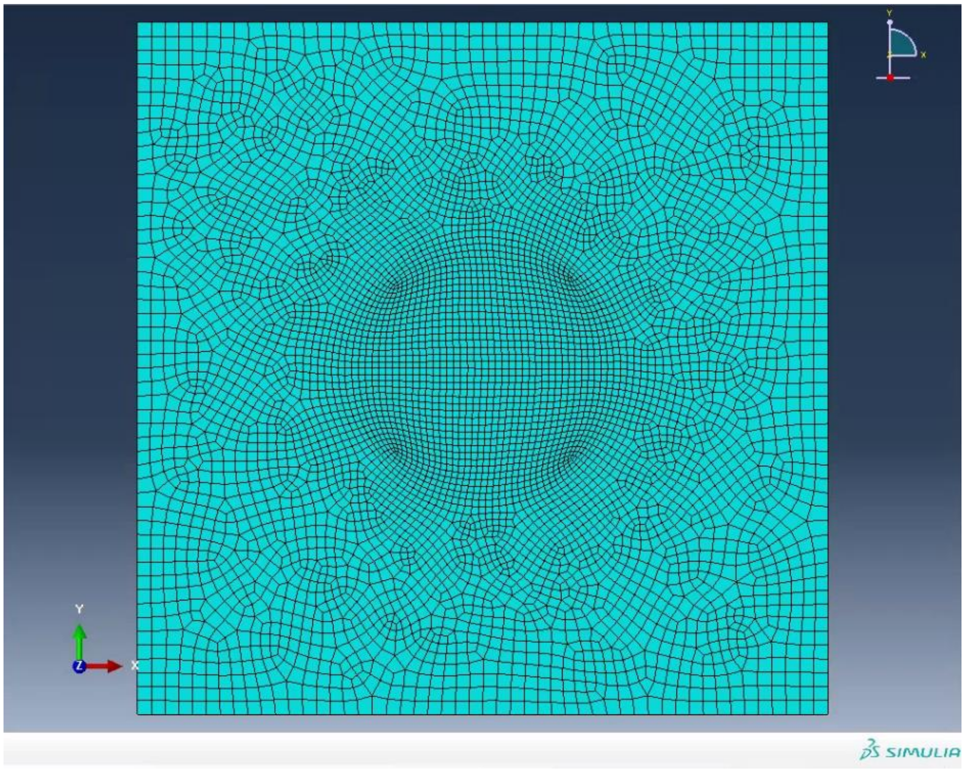

Figure 4.3 Mesh of the plate

4.3 Modeling the projectile

The projectile has been modeled as 3D discrete rigid solid with a diameter of 20 mm, a length 80 mm and a conical nose of altitude 20 mm. A reference point has been designated to represent the body. Mass of the projectile has been to this reference point as point mass/inertia. The mass of the projectile has been assigned as 10 grams.

The projectile has been meshed into a total of 303 R3D4 elements (a 4-node 3-D bilinear rigid quadrilateral element) and 303 nodes. The projectile has been only allowed movement in the Z-direction. The velocity has been assigned to the projectile using a pre-defined field.

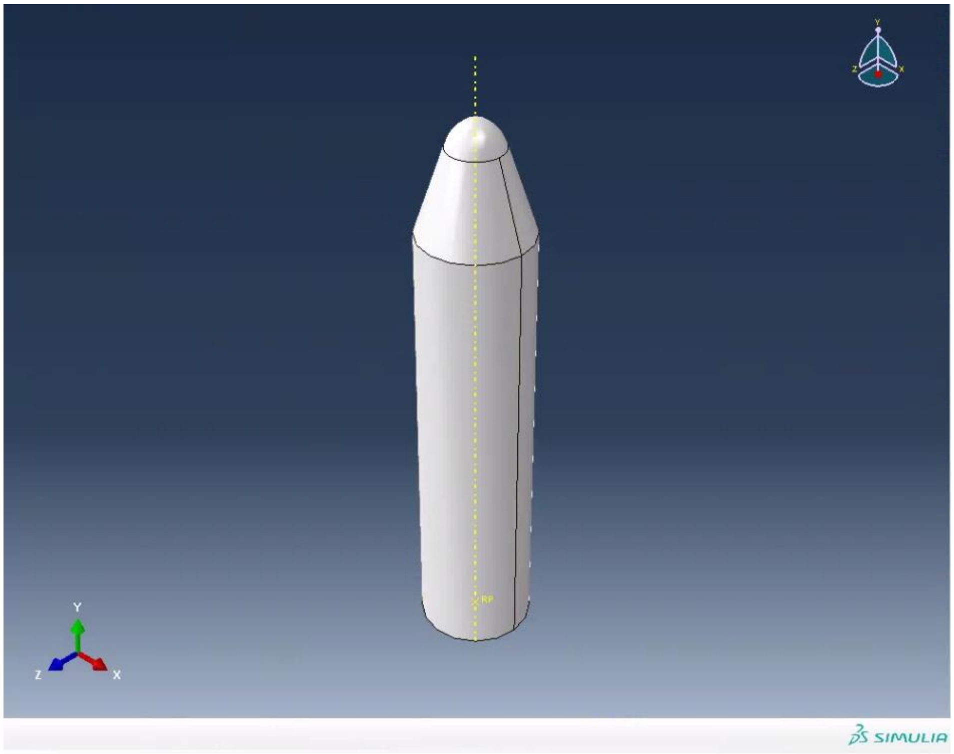

Figure 4.4 3D view of the projectile part

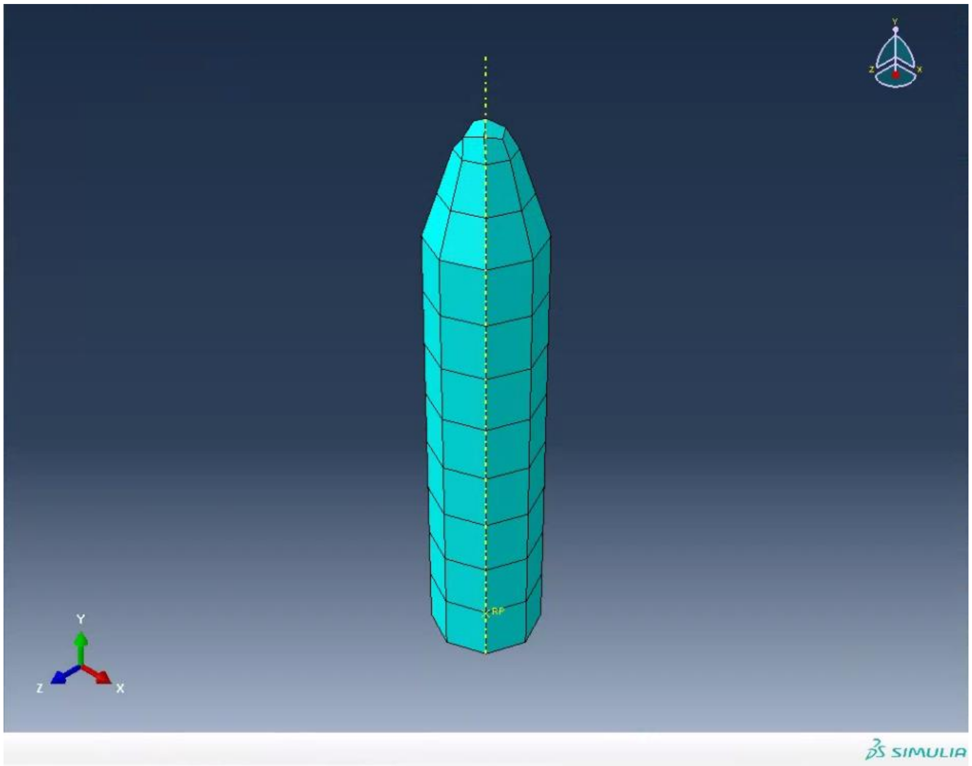

Figure 4.5 Mesh of the projectile

4.4 Modeling the assembly

The plate and the projectile has been assembled under the assembly module and interactions have been defined for the contact. The projectile is placed at a distance of 20 mm away from the plate. Normal Behavior contact property has been defined with “Hard Contact” Pressure-Overclosure relationship and separation after contact has been allowed. A General (Explicit) interaction has been defined for the contact property. A Dynamic, Explicit time step has been created for a duration of 0.001 seconds and with automatic incrementation. Nonlinear geometric effects have been turned on.

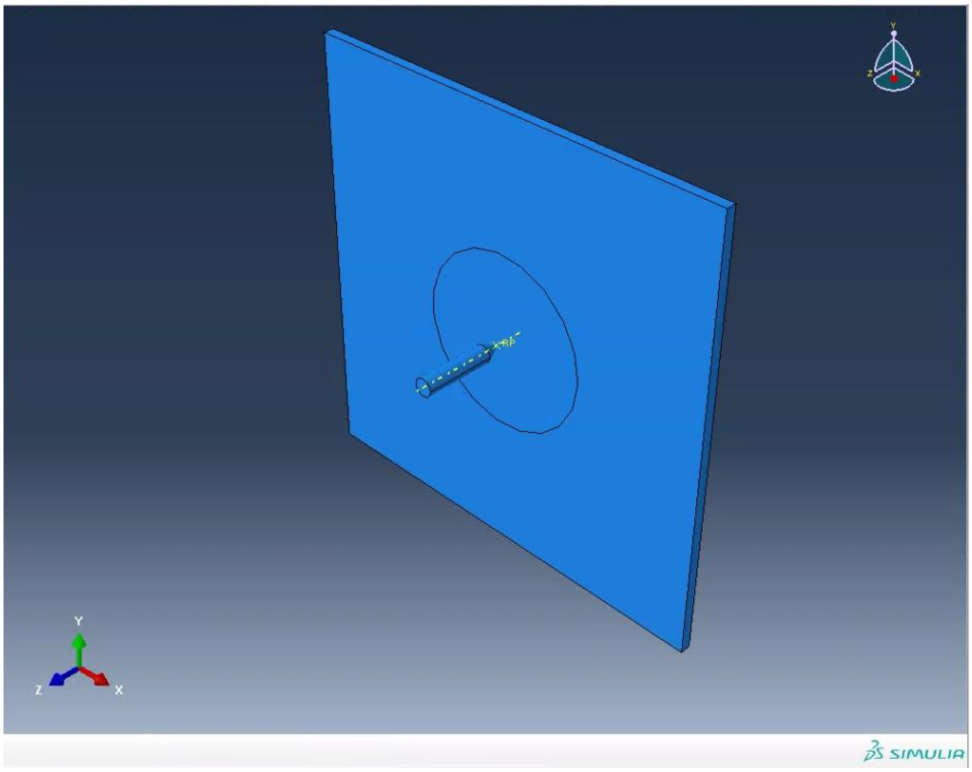

Figure 4.6 Assembly of projectile and plate

4.5 Analysis of the problem

The problem has been analyzed for plate temperatures 20˚C, 200˚C, 400˚C and 600˚C, and projectile velocities 100 m/s, 520 m/s and 800 m/s. While analyzing for different plate temperatures, the projectile velocity was kept at 520 m/s. Similarly, while analyzing for different projectile velocities, the plate temperature was kept at 20˚C. As expected, the stresses and strains were maximum in the central part of the plate near the crack through which the bullet penetrates. However, the stresses and strains developed were different in different cases. The values of applied stress and plastic strains developed were extracted for some elements near the central region of the plate for the calculation of the Damage Evolution Parameter, which has been discussed in the next chapter. The following pictures show the cracks developed for the different cases considered.

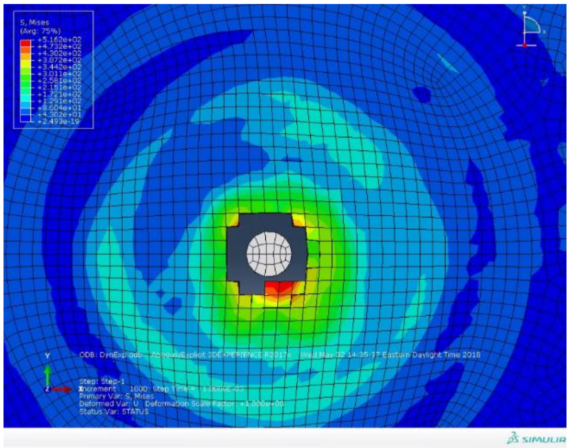

Figure 4.7 (a) Plate 20˚C, projectile 520 m/s

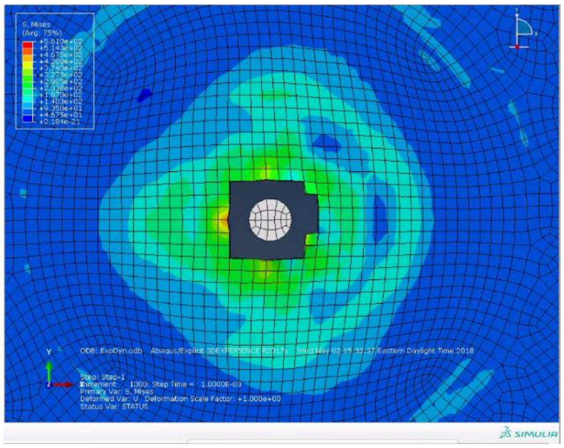

Figure 4.7 (b) Plate 200˚C, projectile 520 m/s

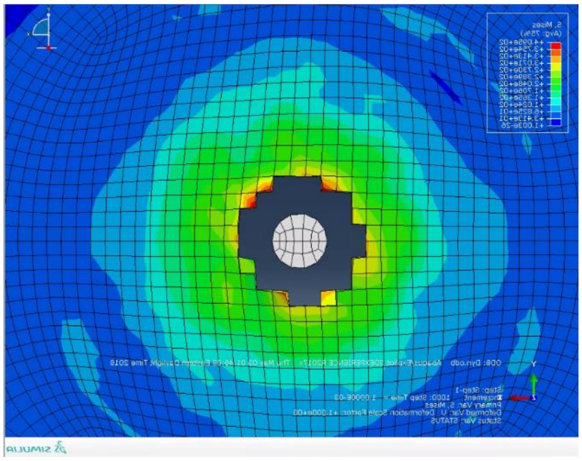

Figure 4.7 (c) Plate 400˚C, projectile 520 m/s

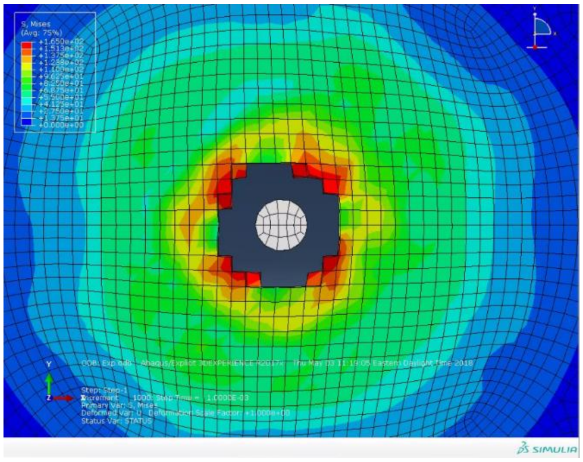

Figure 4.7 (d) Plate 600˚C, projectile 520 m/s

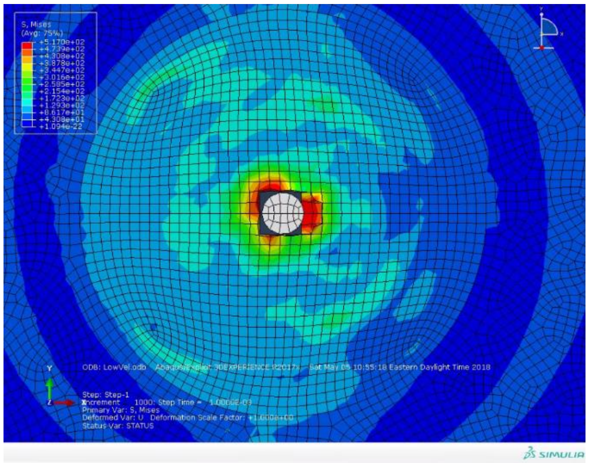

Figure 4.7 (e) Plate 20˚C, projectile 100 m/s

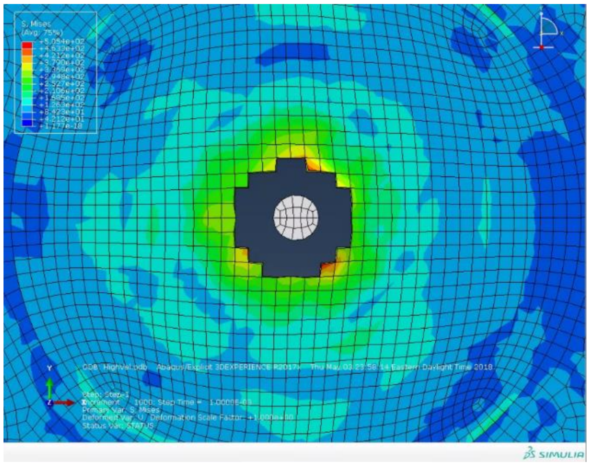

Figure 4.7 (f) Plate 20˚C, projectile 800 m/s

5.0Results and Discussions

5.1 Calculation of Damage Evolution Parameter

For calculation of the Damage Evolution Parameter, first, internal entropy difference is calculated from the applied stress and induced plastic strain values obtained from the numerical simulations using ABAQUS/CAE Explicit. Internal entropy difference is calculated using the simplified form of equation (29) as:

$$\Delta s_i = \int_{t_0}^{t_1} \frac{\sigma : \dot{\varepsilon}^p}{\rho T}\, dt \tag{30}$$

It is assumed that heat generation is small compared to plastic work. This is because only the effects of mechanical load of the projectile have been taken into account. Furthermore, the load is uniaxial, so the problem gets reduced to one direction only. Therefore, the plastic work is the product of applied stress and induced plastic strain. For the purpose of numerical computation, equation (30) is simplified as:

$$\Delta s_i = \sum \frac{(\sigma^* \Delta \varepsilon^p)}{\rho T} \tag{324}$$

The Damage Evolution Parameter has been calculated using equation (27). The value of this Damage Evolution Parameter has been then plotted against time in seconds to obtain the Damage Evolution Curves which have been used to compare the different cases of plate temperature and projectile velocity.

The analyses have been run for a total time duration of 0.001 seconds. Since ballistic impact is an instantaneous phenomenon, damage occurs within extremely small periods of time. Data has been extracted for time increments of 1 microsecond (10^{-6} seconds) for elements in the central part of the plate, which will be most affected. The Damage Evolution Parameter goes from 0 to 1 directly because high amounts of stresses and strains are developed within extremely short time intervals. The stress-strain curves for the selected elements have been shown in Appendix-B.

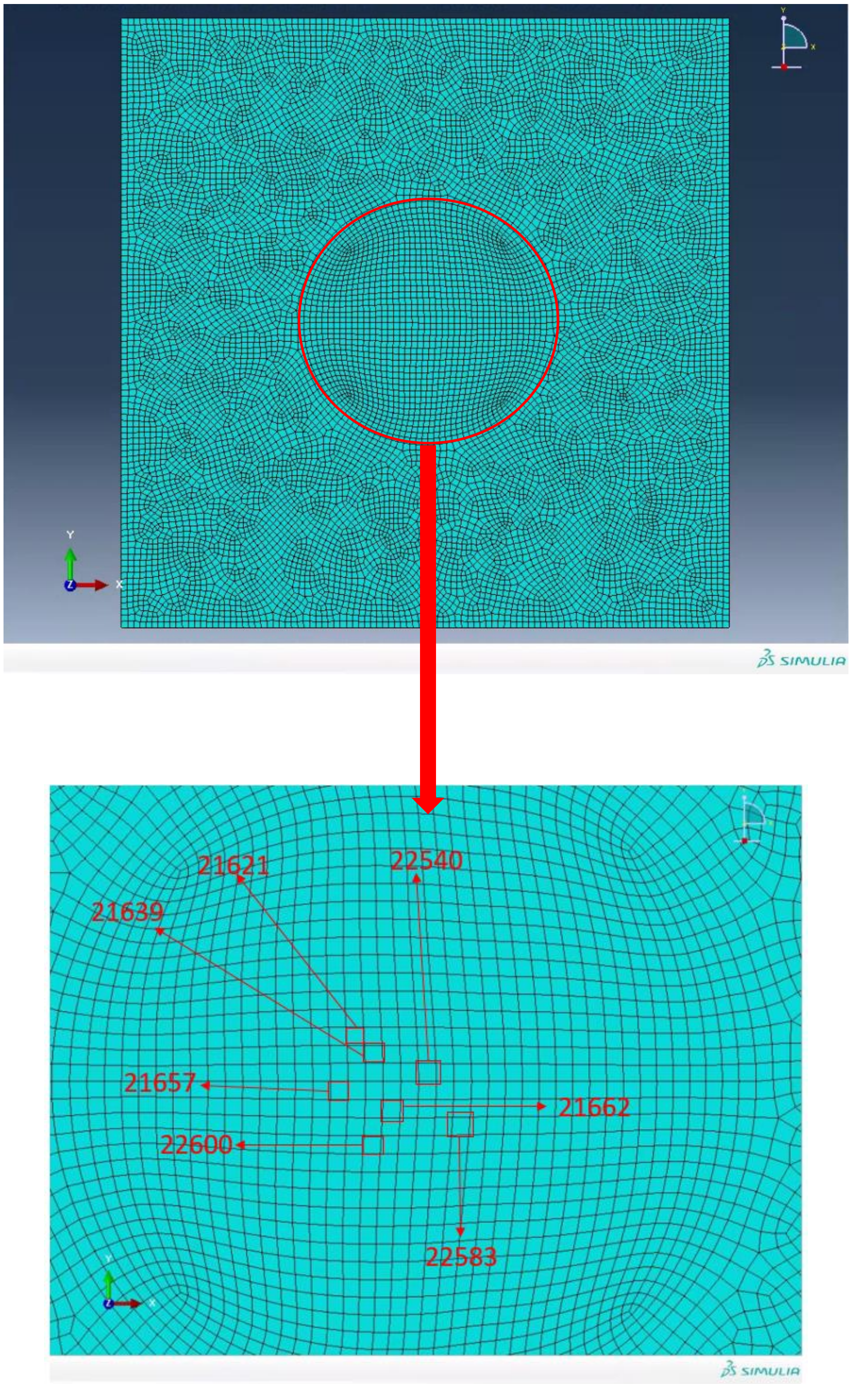

Figure 5.1 Elements for which Damage Evolution Curves have been generated

5.2 Damage Evolution Curves for different plate temperatures

The problem has been analyzed for plate temperatures at 20˚C, 200˚C, 400˚C and 600˚C. The projectile velocity has been considered to be 520 m/s for all four cases. Damage Evolution Curves are generated for elements 21657, 21662, 22600 and 22583.

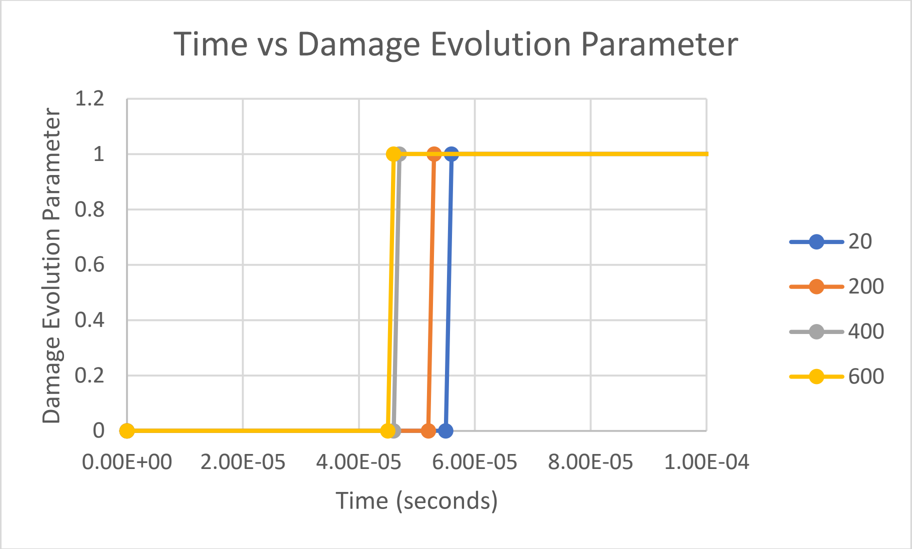

Figure 5.2 (a) Damage Evolution Curve for element 21657

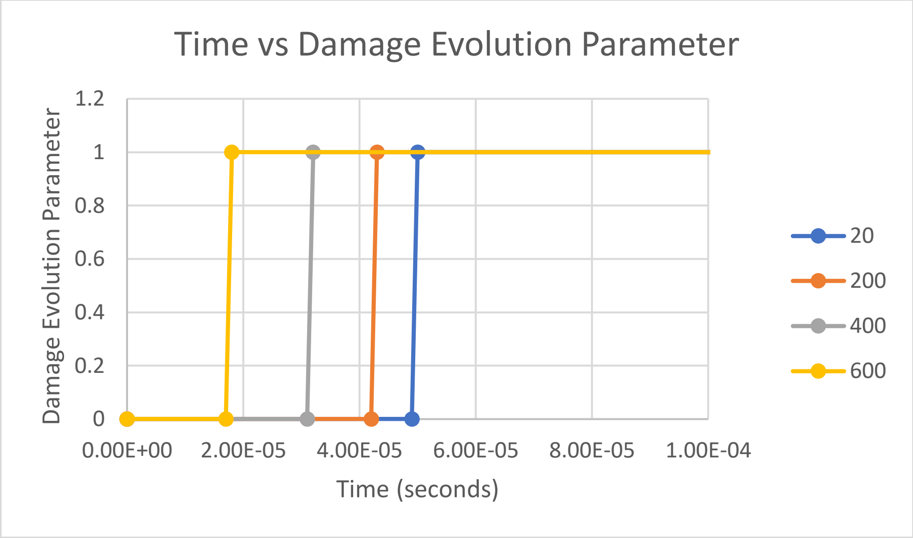

Figure 5.2 (b) Damage Evolution Curve for element 21662

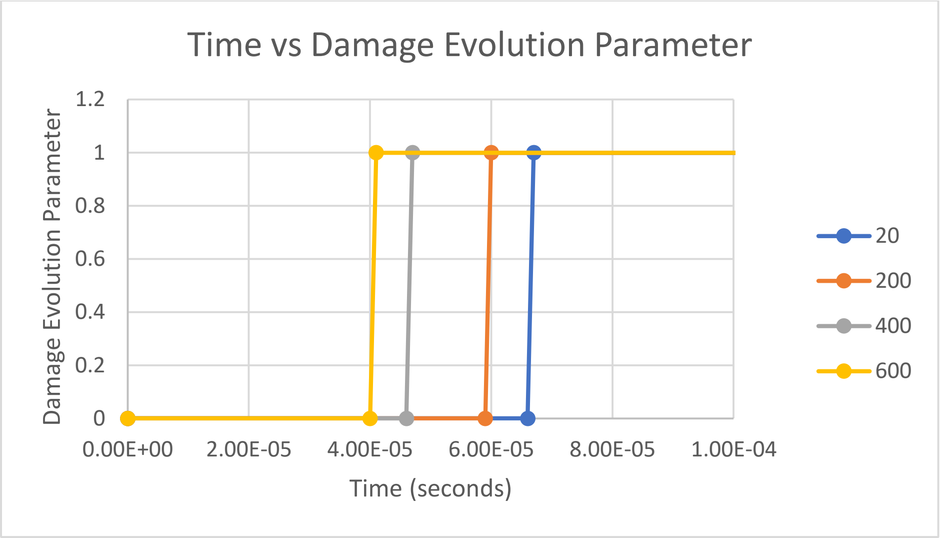

Figure 5.2 (c) Damage Evolution Curve for element 22600

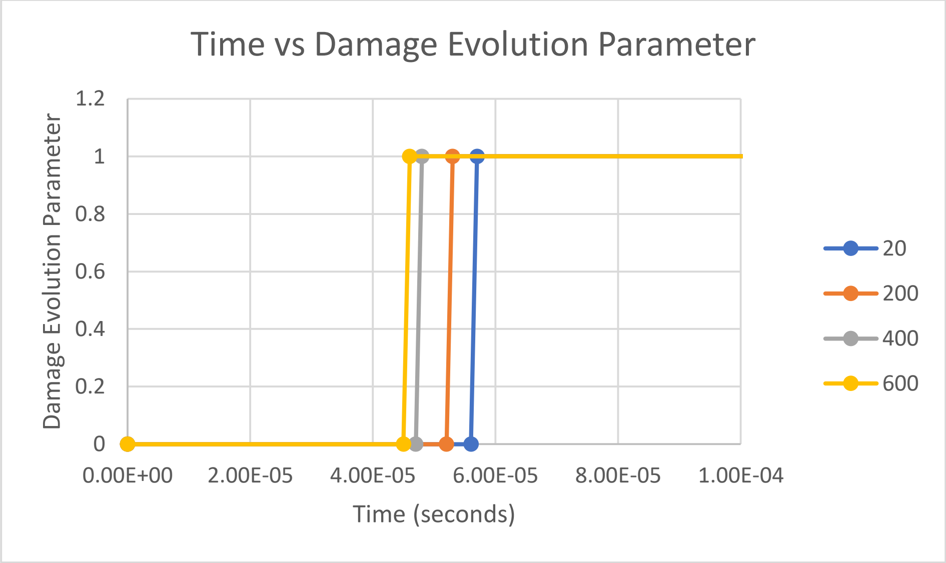

Figure 5.2 (d) Damage Evolution Curve for element 22583

It can be seen from the above Damage Evolution Curves that damage takes place sooner when the plate temperature is higher. This is because at elevated temperatures plastic deformation occurs more easily. The tensile strength, yield strength and modulus of elasticity decrease with increasing temperature.

5.3 Damage Evolution Curves for different projectile velocities

Analyses have been carried out for projectile velocities 100 m/s, 520 m/s and 800 m/s. The plate temperature has been considered to be 20˚C for all three cases. Damage Evolution Curves have been generated for elements 21621, 21639, 22540 and 22600.

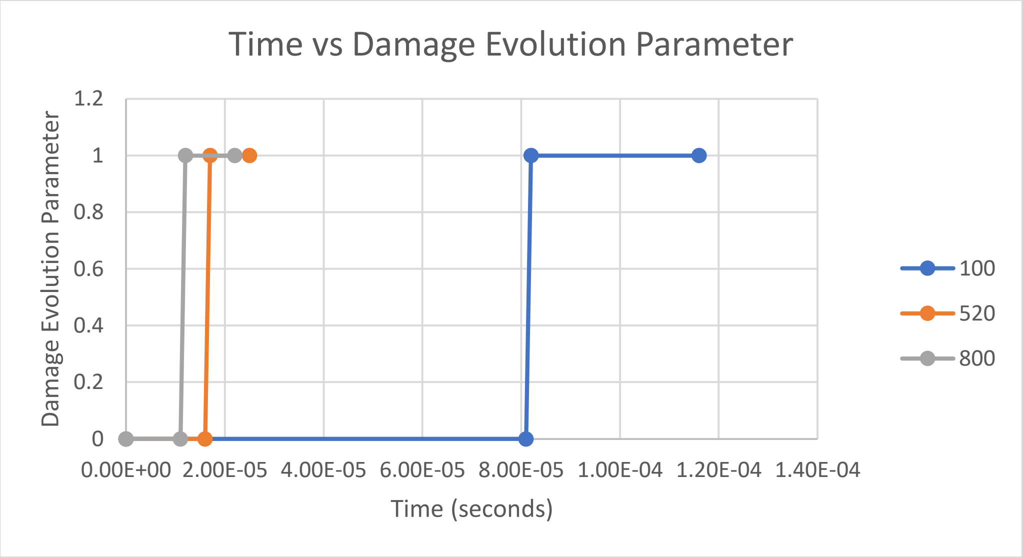

Figure 5.3 (a) Damage Evolution Curve for element 21621

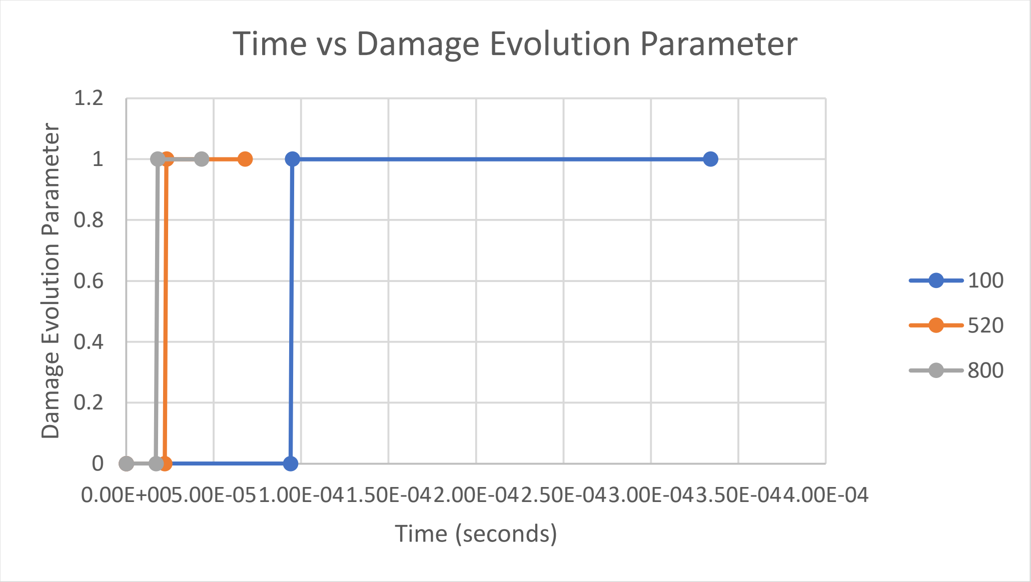

Figure 5.3 (b) Damage Evolution Curve for element 21639

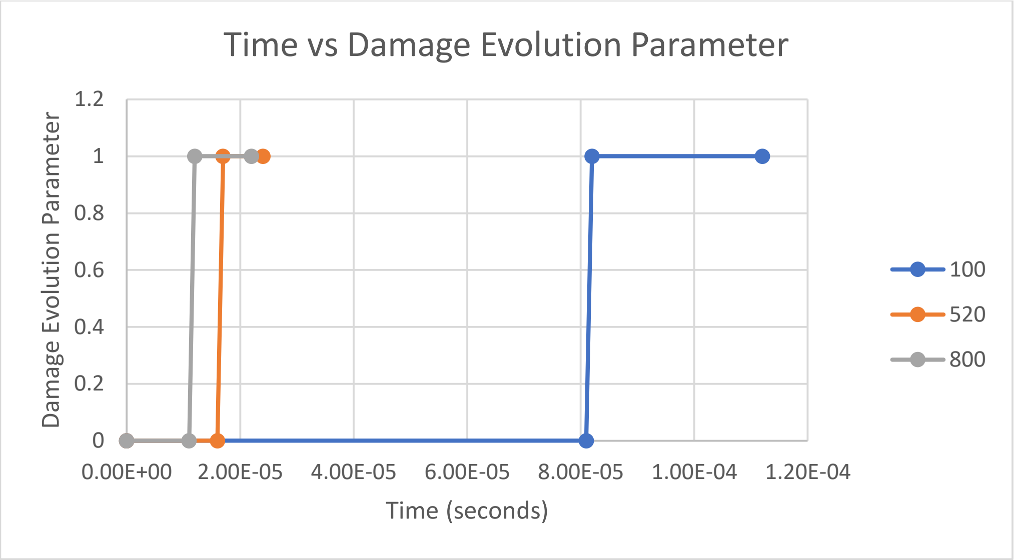

Figure 5.3 (c) Damage Evolution Curve for element 22540

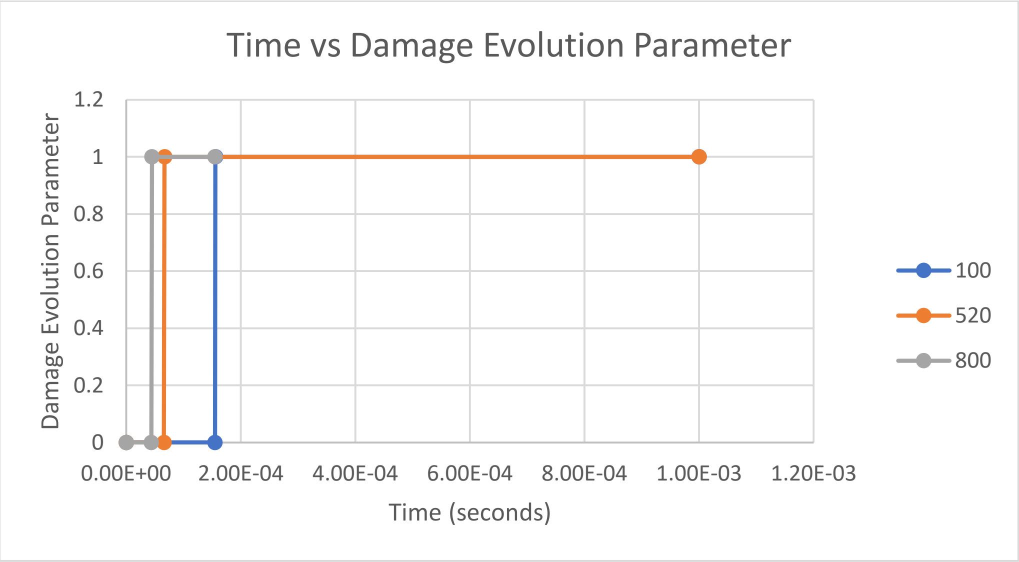

Figure 5.3 (d) Damage Evolution Curve for element 22600

It can be seen from the above curves that the higher the projectile velocity, the sooner the damage occurs. Also, as the speed of projectile goes on increasing, the time period at which damage occurs decreases exponentially. This trend can be visualized in the following projectile velocity vs damage initiation time curve.

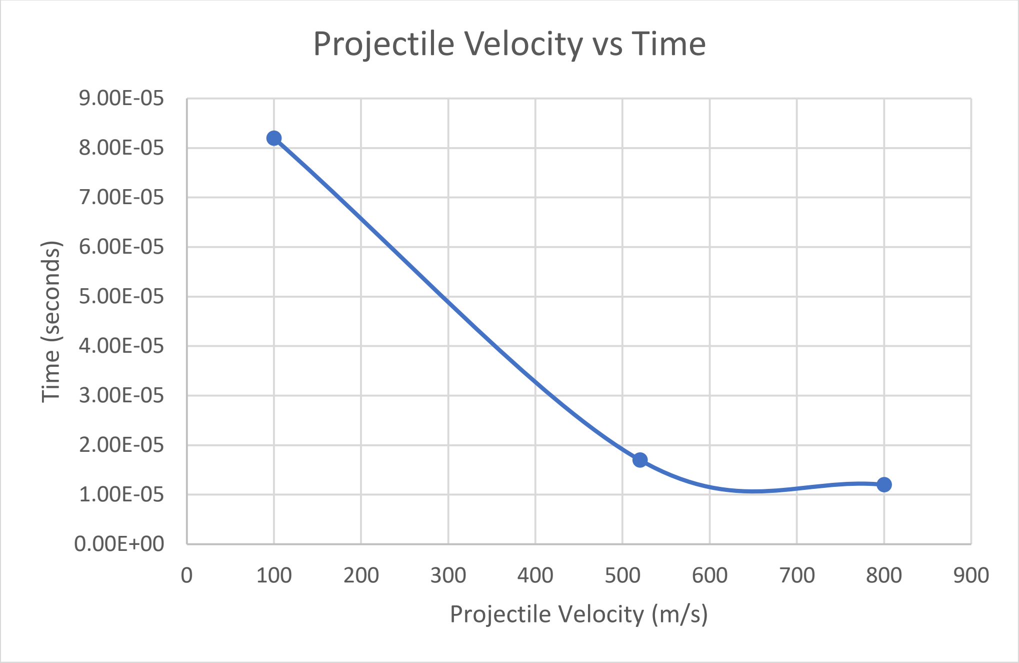

Figure 5.4 (a) Projectile Velocity vs Time for element 21621

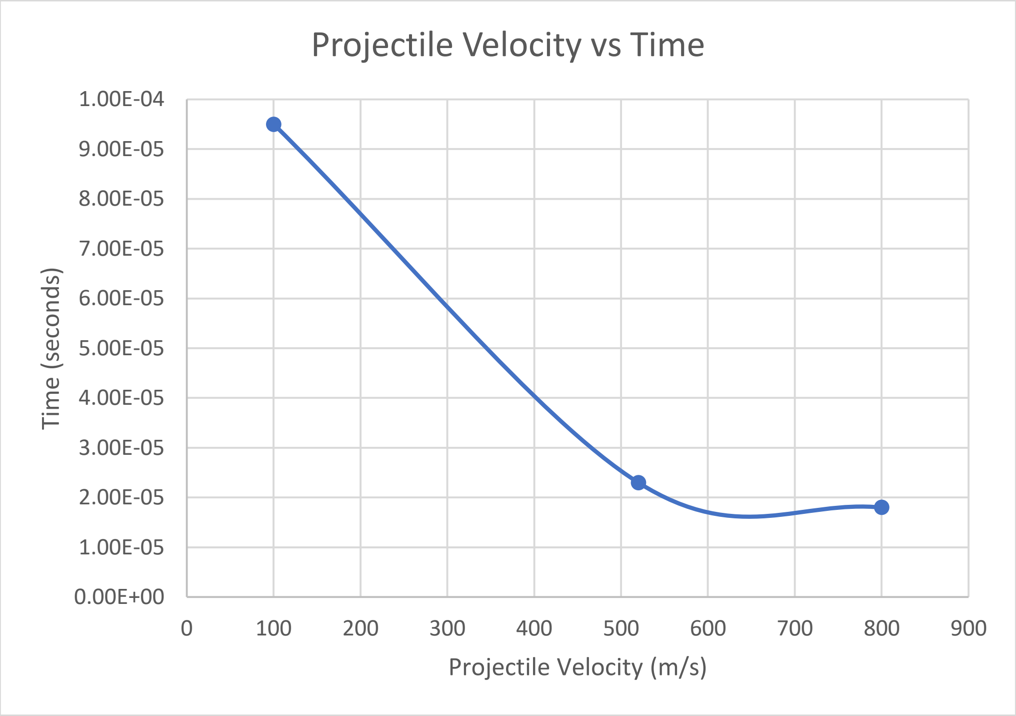

Figure 5.4 (b) Projectile Velocity vs Time for element 21639

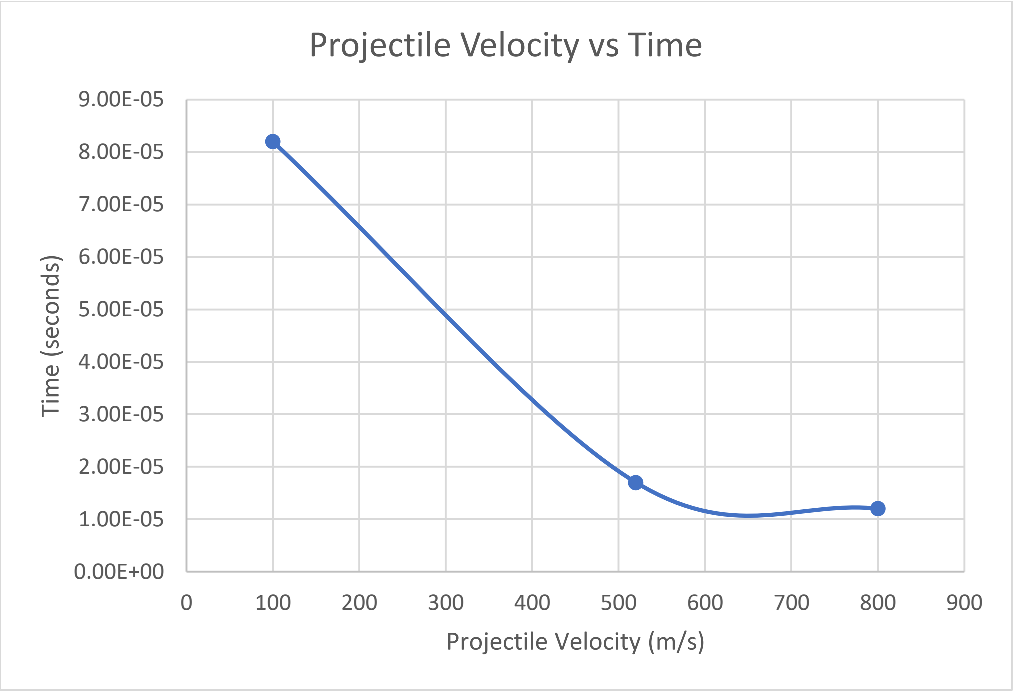

Figure 5.4 (c) Projectile Velocity vs Time for element 22540

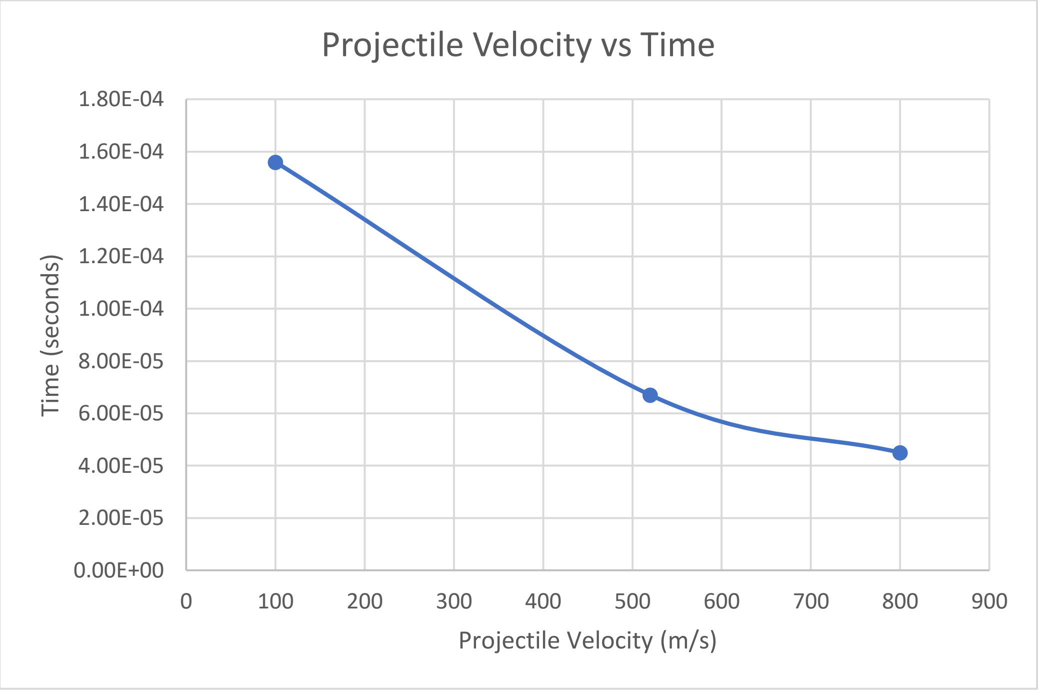

Figure 5.4 (d) Projectile Velocity vs Time for element 22600

6.0 Conclusions

Ballistic Impact has been studied for an A36 Steel plate using the New Unified Mechanics Theory. The study has been carried out for plate temperatures of 20˚C, 200˚C, 400˚C and 600˚C and for projectile velocities 100 m/s, 520 m/s and 800 m/s. Modeling and analysis has been done using ABAQUS/CAE Explicit FE Package. The values of applied stress and induced plastic strain obtained from these numerical simulations are then used to calculate the internal entropy difference and eventually, the Damage Evolution Parameter. Damage Evolution Curves are then obtained by plotting the Damage Evolution Parameter against time, which are used to compare the trends for different plate temperatures and different projectile velocities.

It was observed that in case of varying plate temperature, damage takes place sooner when the plate temperature is higher. In case of varying projectile velocity, it was observed that the higher the projectile velocity, the sooner the damage occurs. Also, it is seen that the time at which damages occurs decreases exponentially with increase in projectile velocity. These results are in agreement with the trends observed by several researchers from their experimental studies on ballistic impact for cases of varying projectile velocities and target temperatures.

The objective of this work is to study ballistic impact using the New Unified Mechanics Theory. Based on the conclusions of this study and their conformity with the conclusions of experimental results of ballistic impact performed by several researchers, it can be said that the New Unified Mechanics Theory can be used to study ballistic impact. This theory is advantageous over other models because only entropy generation is used as a metric of damage evolution and it does not require any curve fitting techniques. It can also be applied to a wide range of damage problems, for any type of material and any system.

APPENDIX-A

A.1 Temperature-dependent properties of A36 Steel

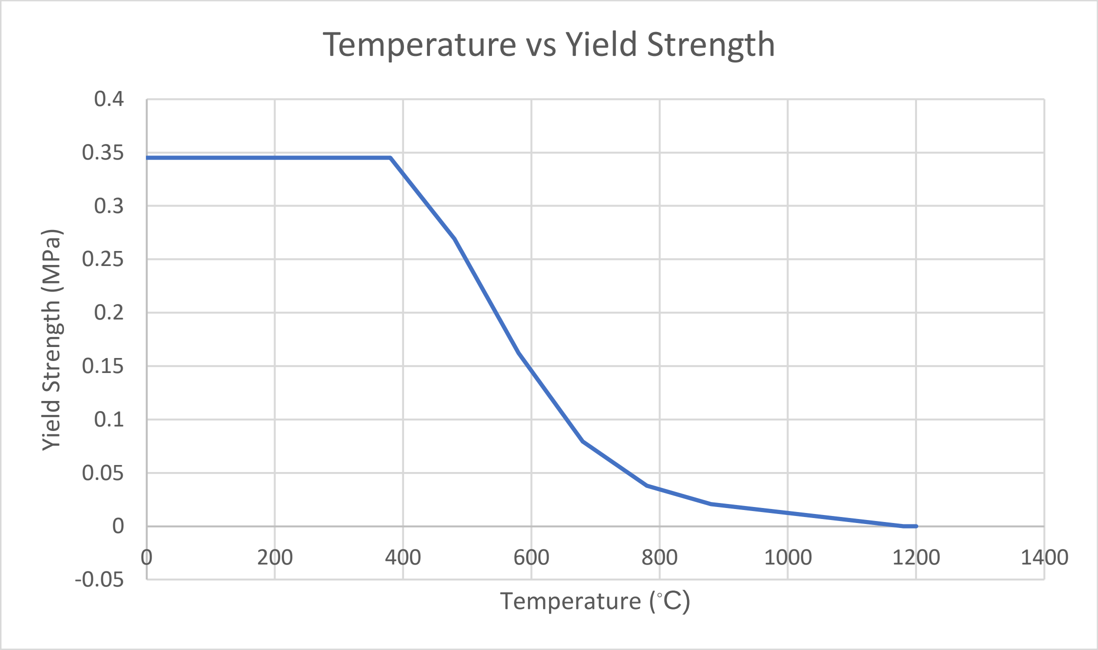

Figure A.1 Variation of Yield Strength with Temperature for A36 Steel

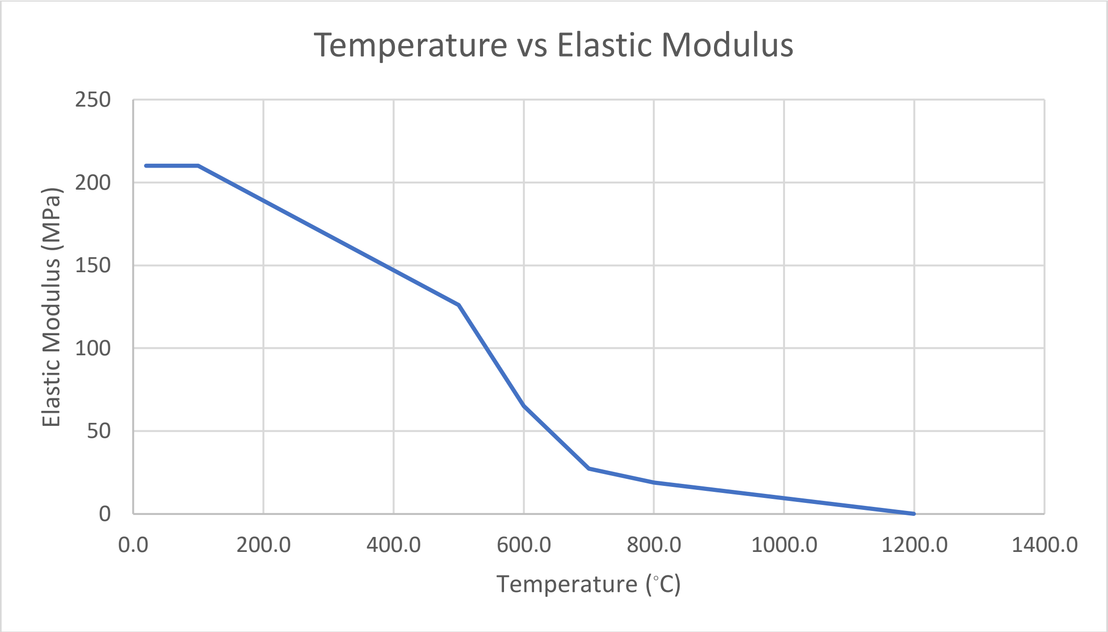

Figure A.2 Variation of Elastic Modulus with Temperature for A36 Steel

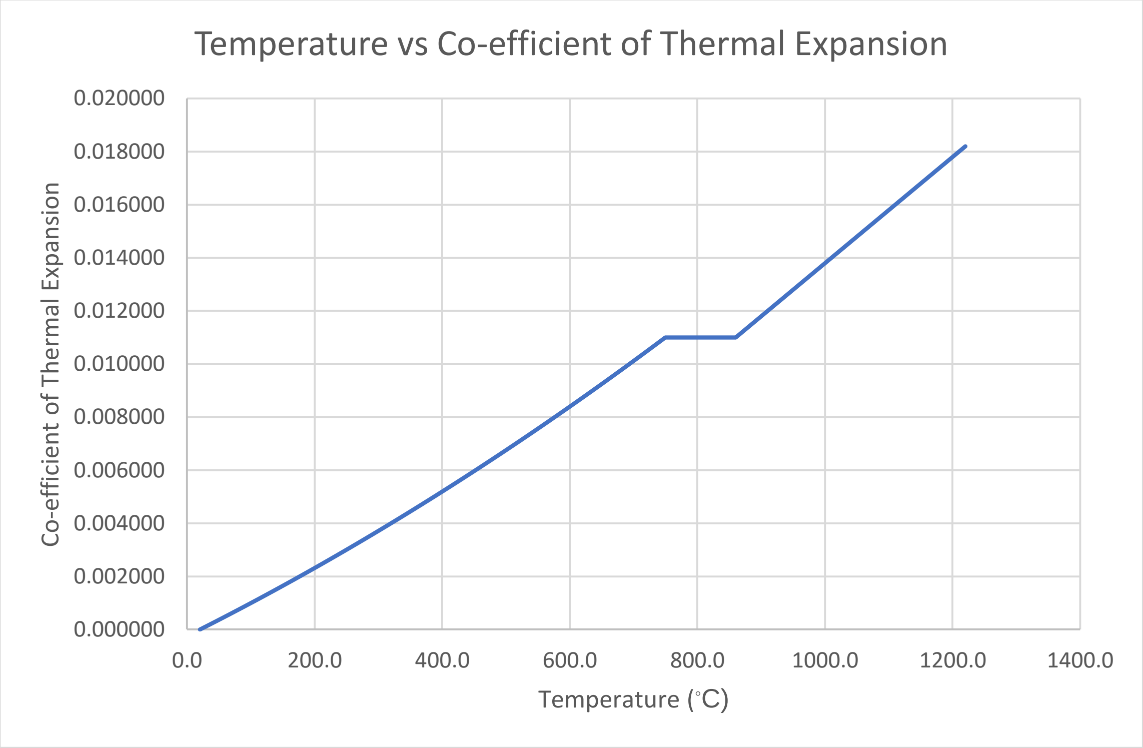

Figure A.3 Variation of Elastic Modulus with Temperature for A36 Steel

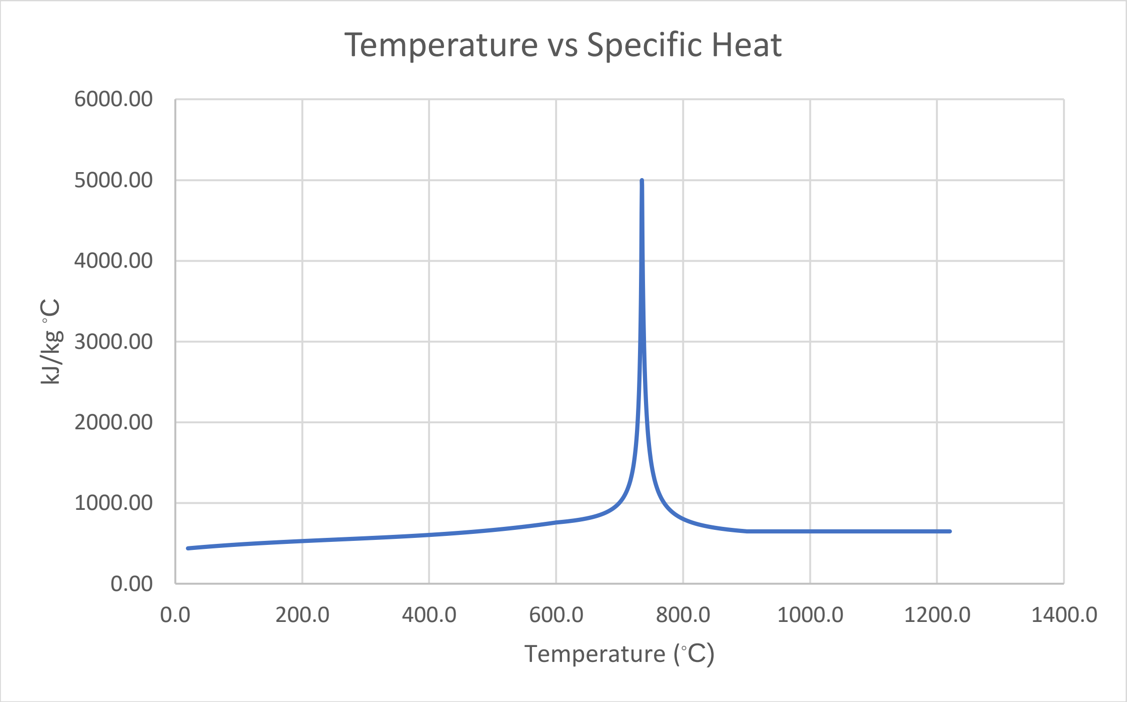

Figure A.4 Variation of Specific Heat with Temperature for A36 Steel

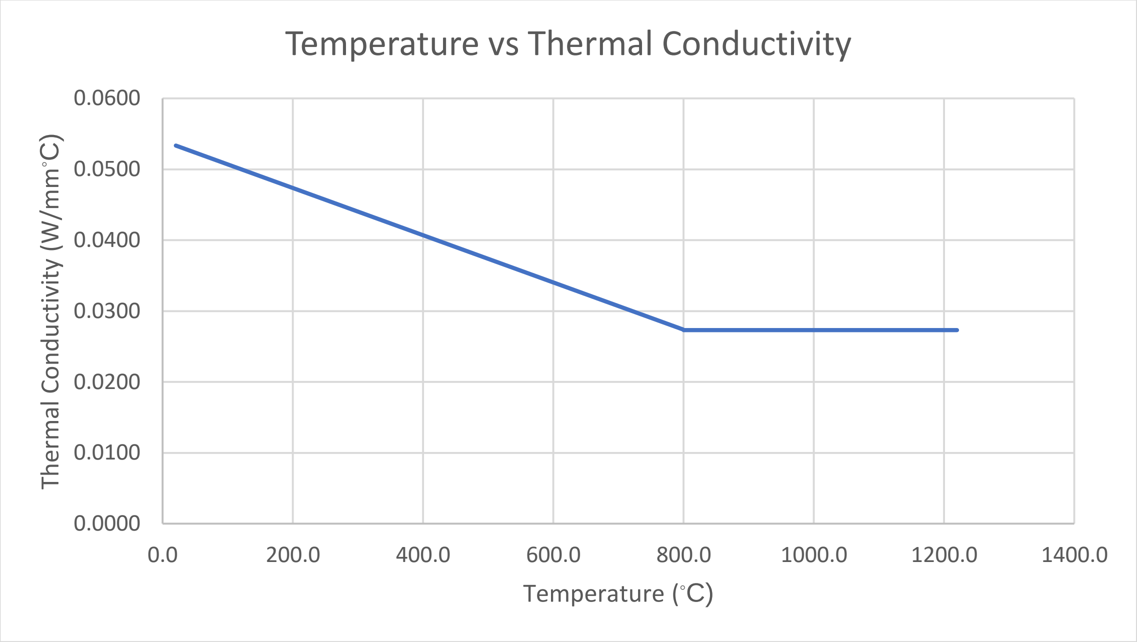

Figure A.5 Variation of Thermal Conductivity with Temperature for A36 Steel

A.2 Temperature-dependent stress strain curves for A36 Steel

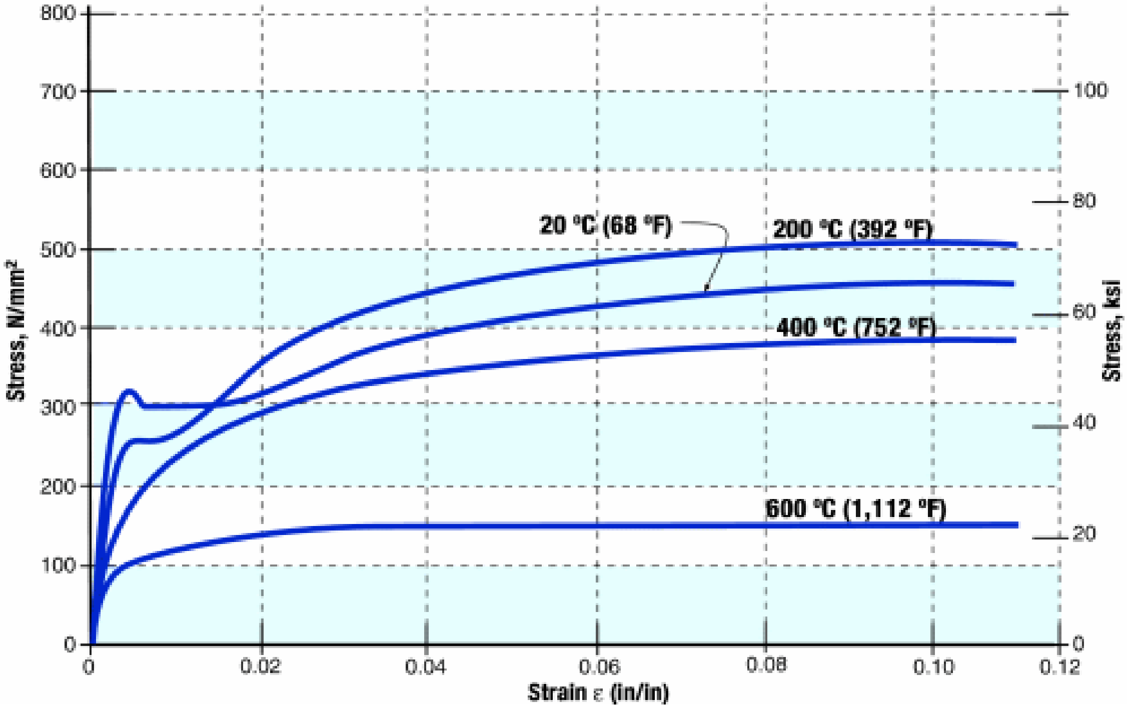

Figure A.6 Stress-Strain curves for A36 Steel at different temperatures

(Milke, Kodur et al. 2002)

APPENDIX-B

B.1 Stress-Strain Curves for Elements studied for varying plate temperature*

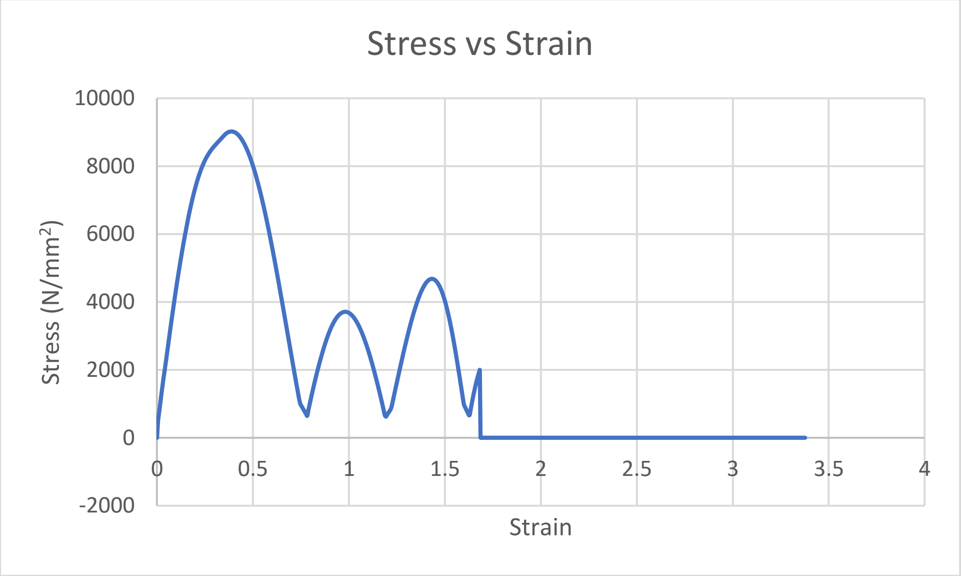

Figure B.1 (a) Element 21657; plate temperature 20˚C

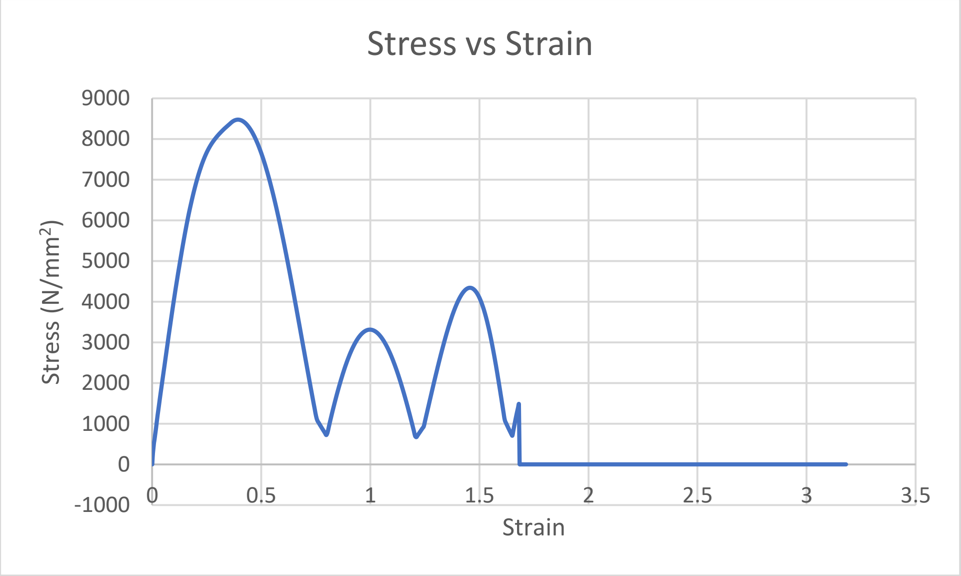

Figure B.1 (b) Element 21657; plate temperature 200˚C

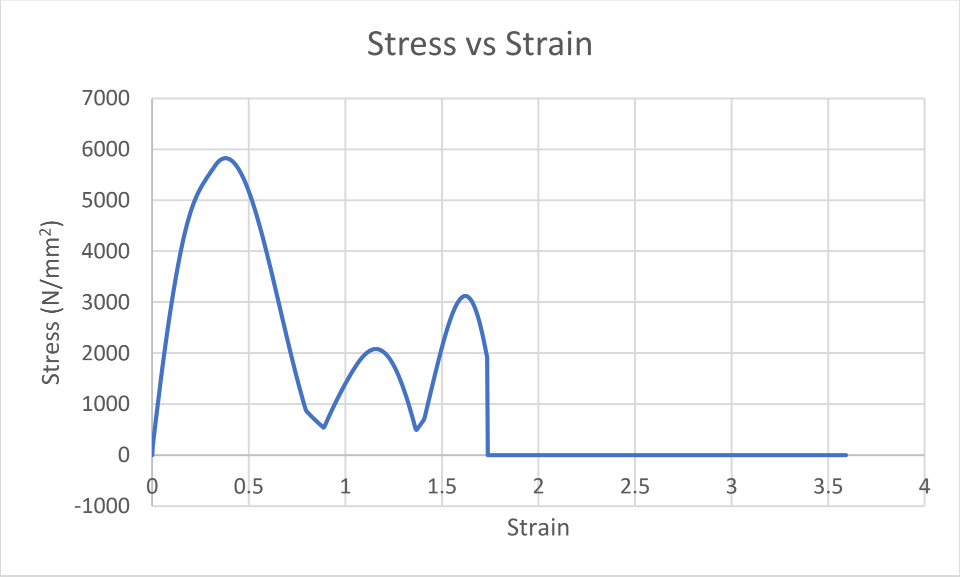

Figure B.1 (c) Element 21657; plate temperature 400˚C

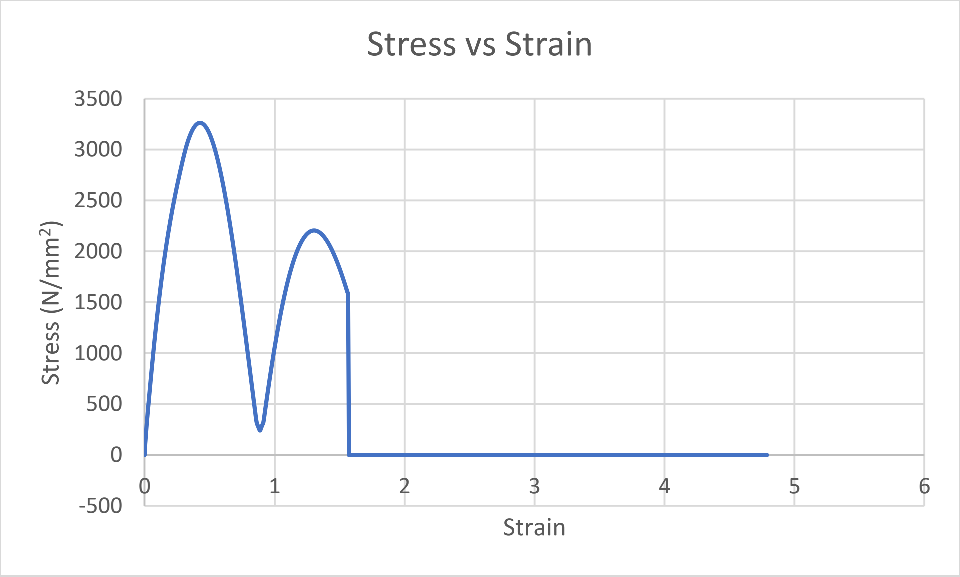

Figure B.1 (d) Element 21657; plate temperature 600˚C

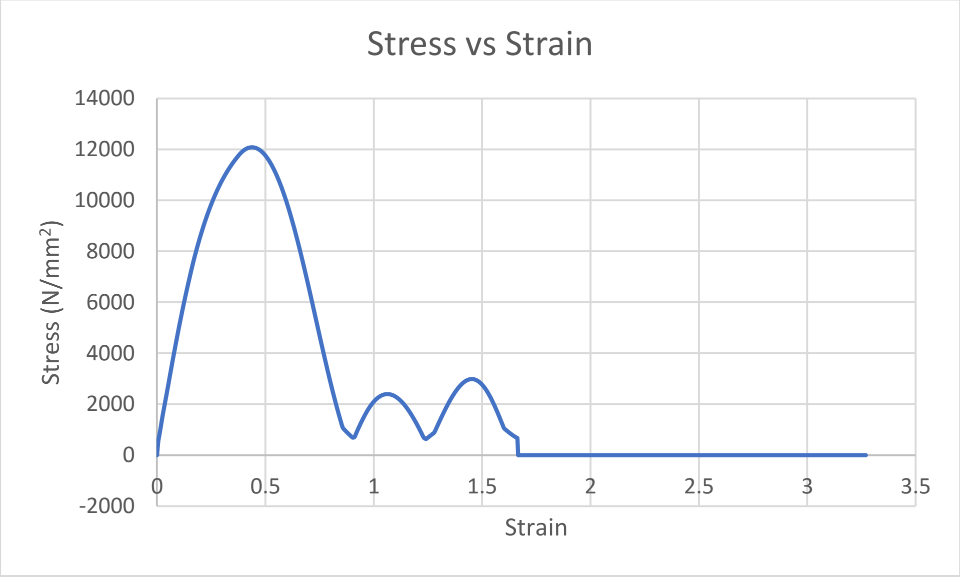

Figure B.2 (a) Element 21662; plate temperature 20˚C

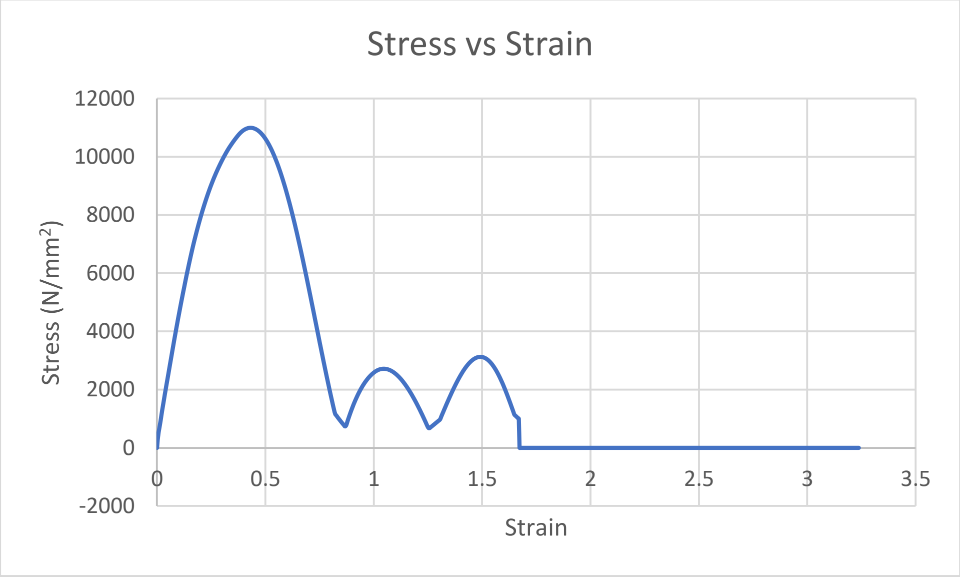

Figure B.2 (b) Element 21662; plate temperature 200˚C

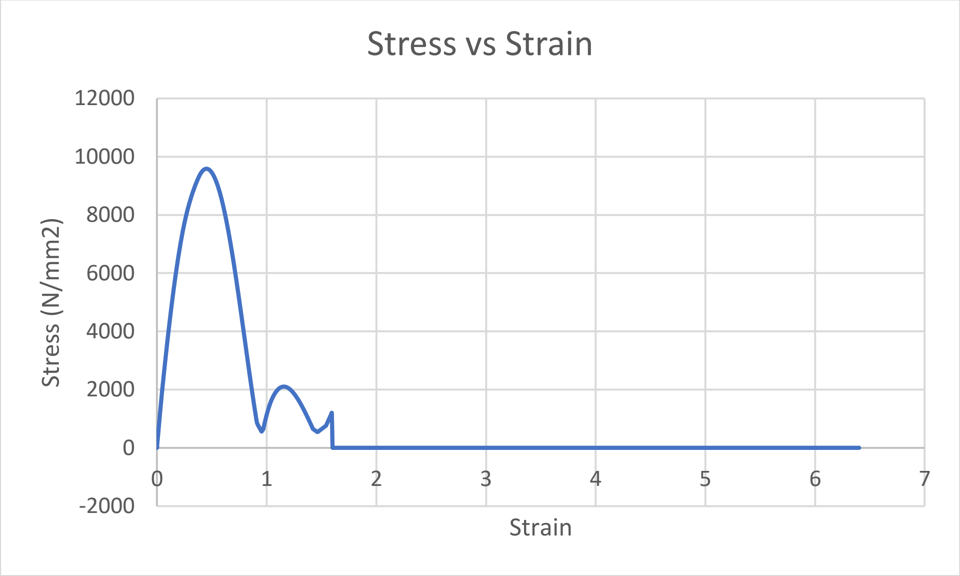

Figure B.2 (c) Element 21662; plate temperature 400˚C

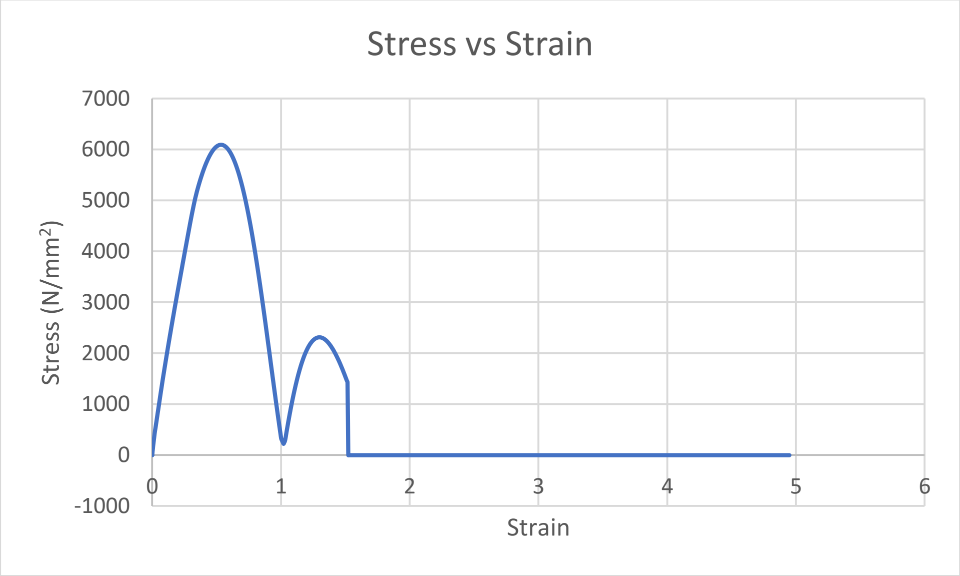

Figure B.2 (d) Element 21662; plate temperature 600˚C

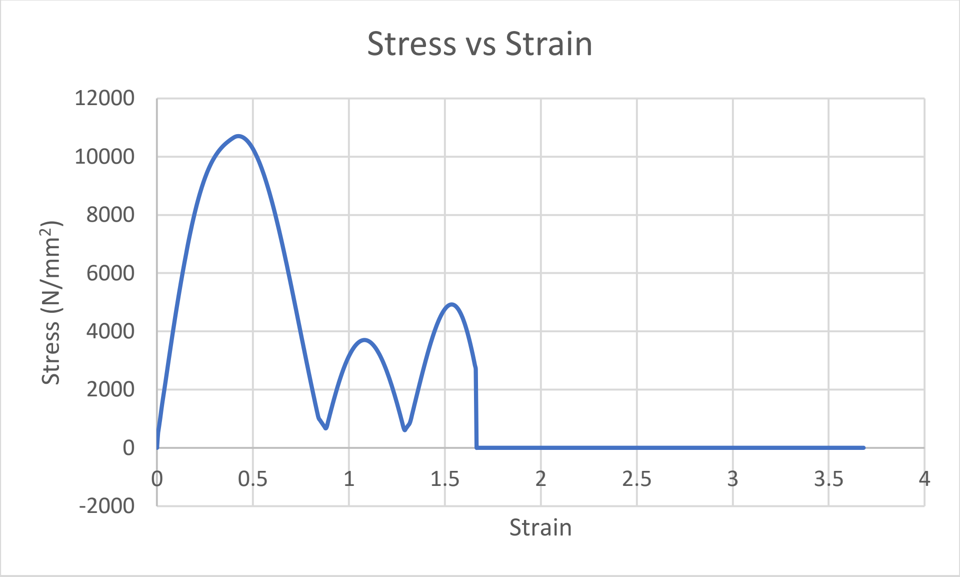

Figure B.3 (a) Element 22583; plate temperature 20˚C

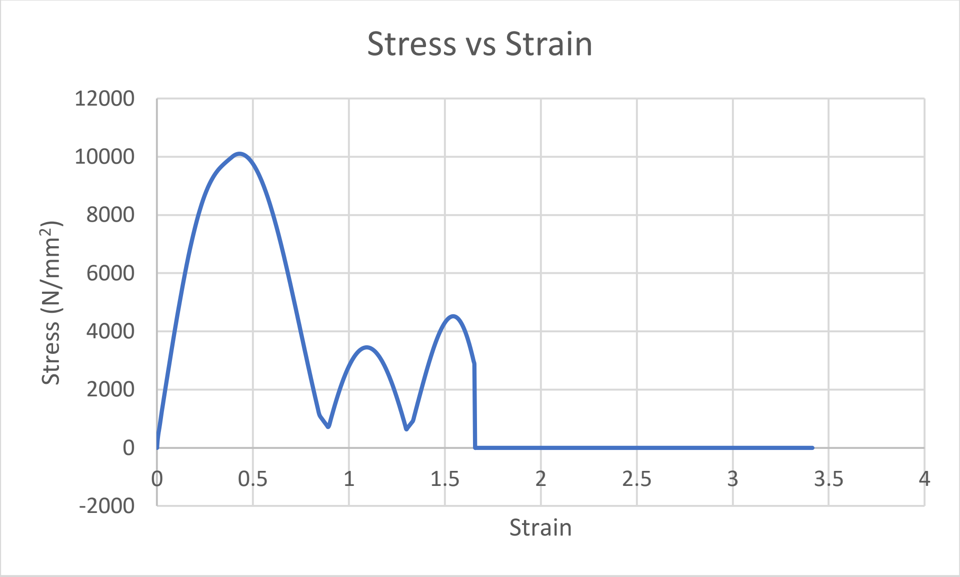

Figure B.3 (b) Element 22583; plate temperature 200˚C

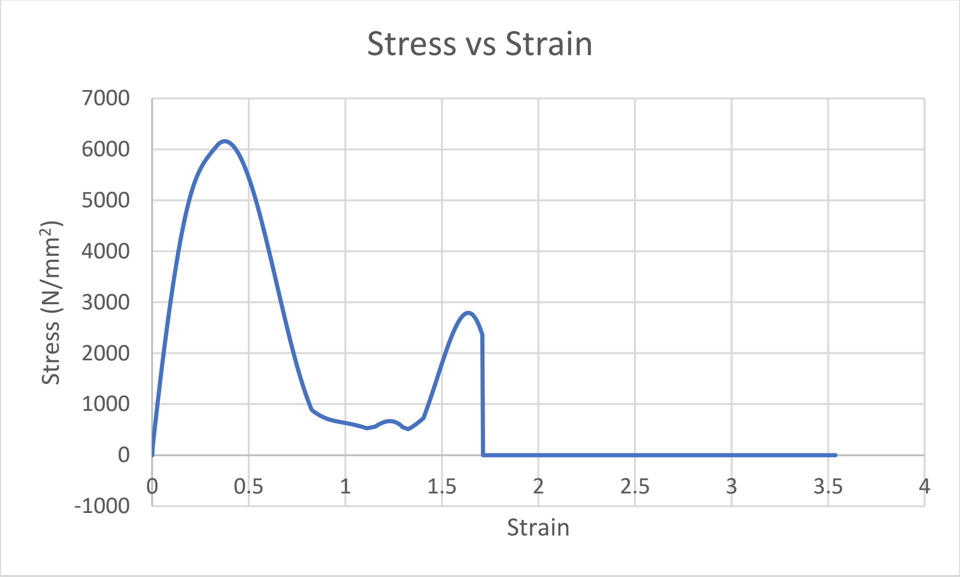

Figure B.3 (c) Element 22583; plate temperature 400˚C

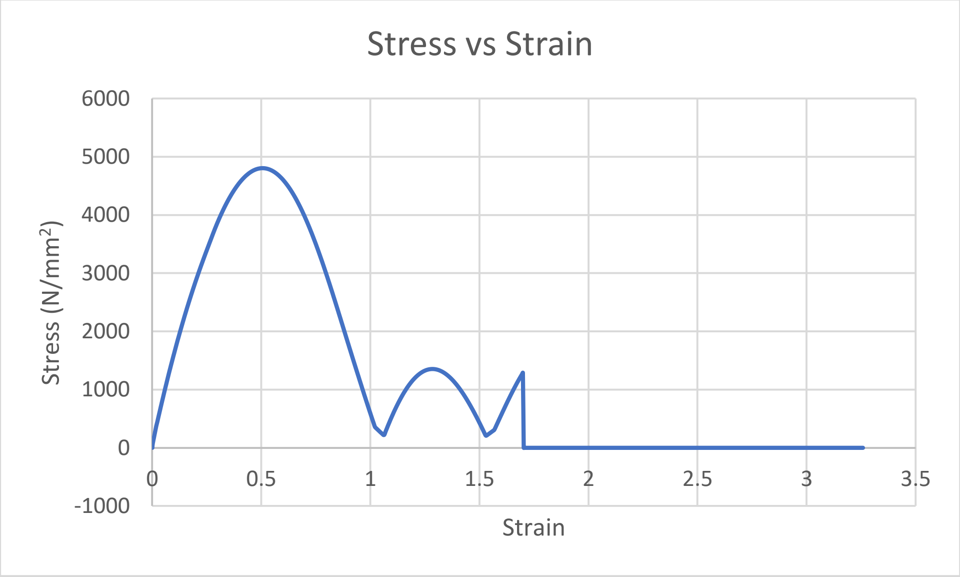

Figure B.3 (d) Element 22583; plate temperature 600˚C

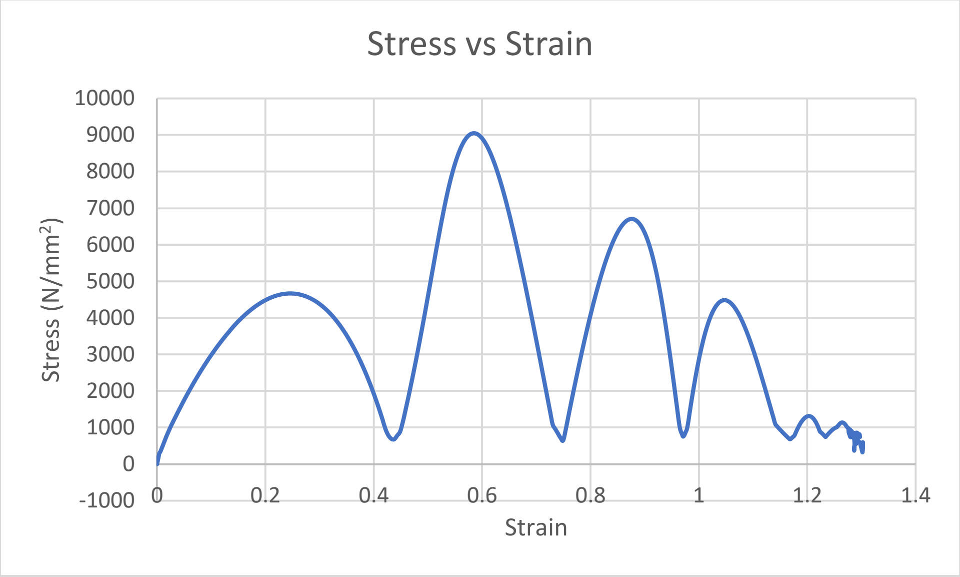

Figure B.4 (a) Element 22600; plate temperature 20˚C

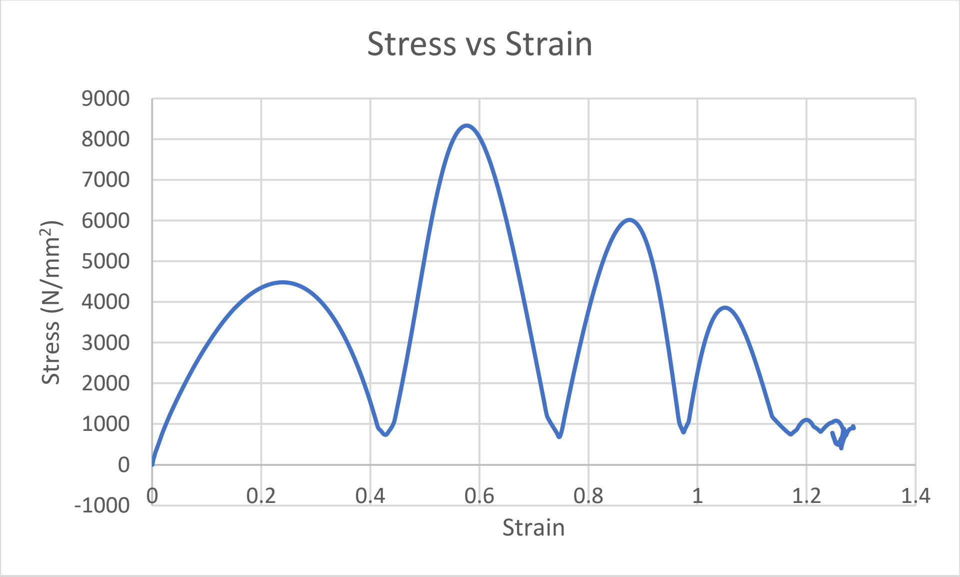

Figure B.4 (b) Element 22600; plate temperature 200˚C

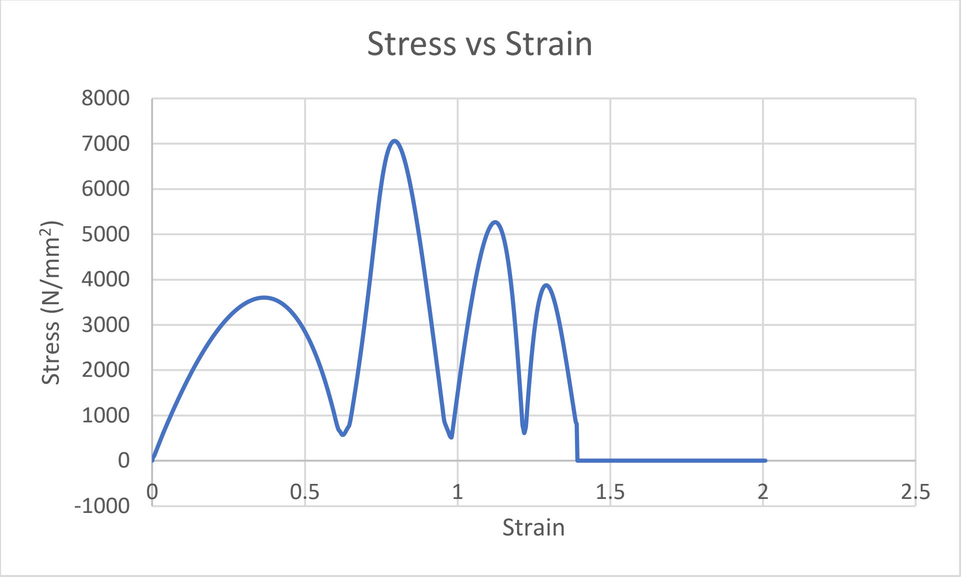

Figure B.4 (c) Element 22600; plate temperature 400˚C

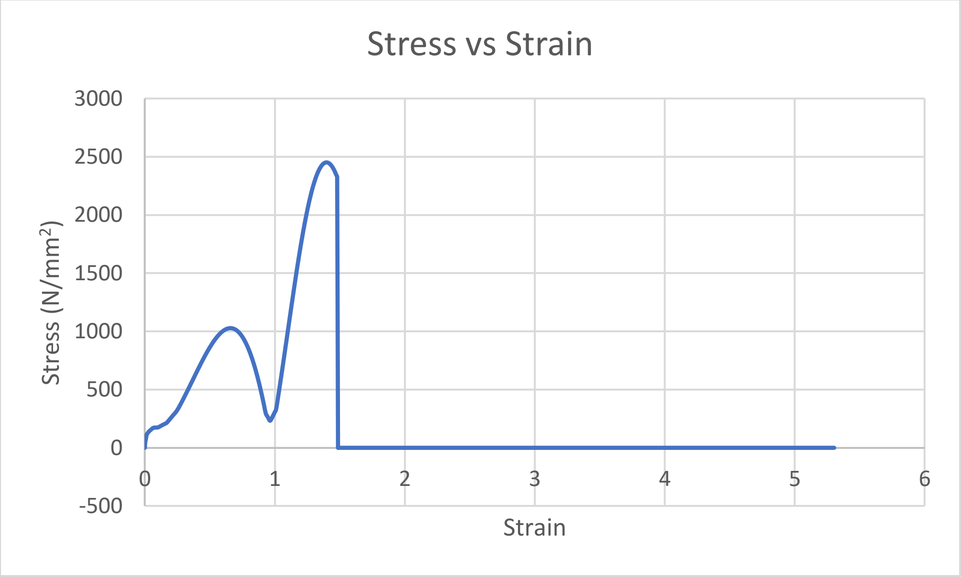

Figure B.4 (d) Element 22600; plate temperature 600˚C

B.2 Stress-Strain Curves for Elements studied for varying projectile velocity*

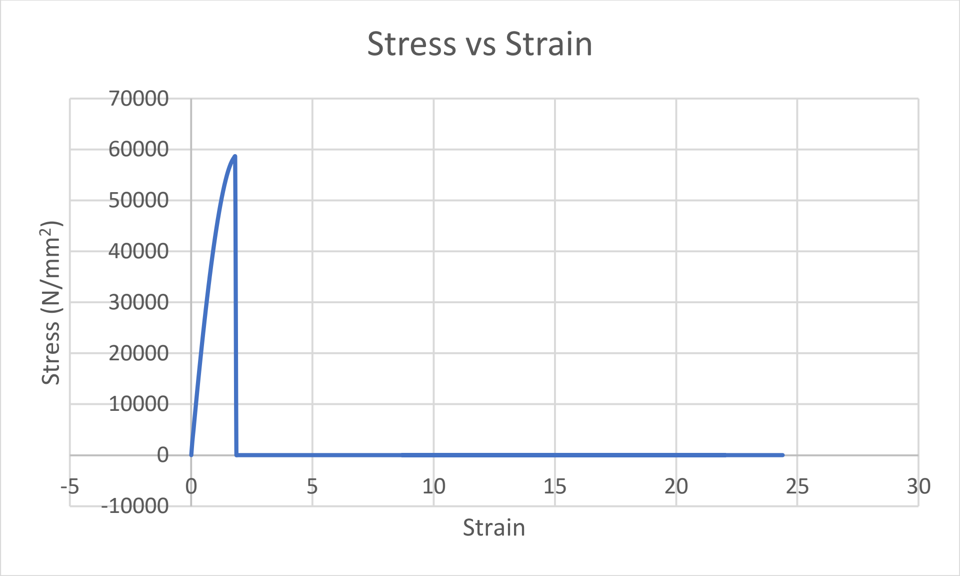

Figure B.5 (a) Element 21621; projectile velocity 100 m/s

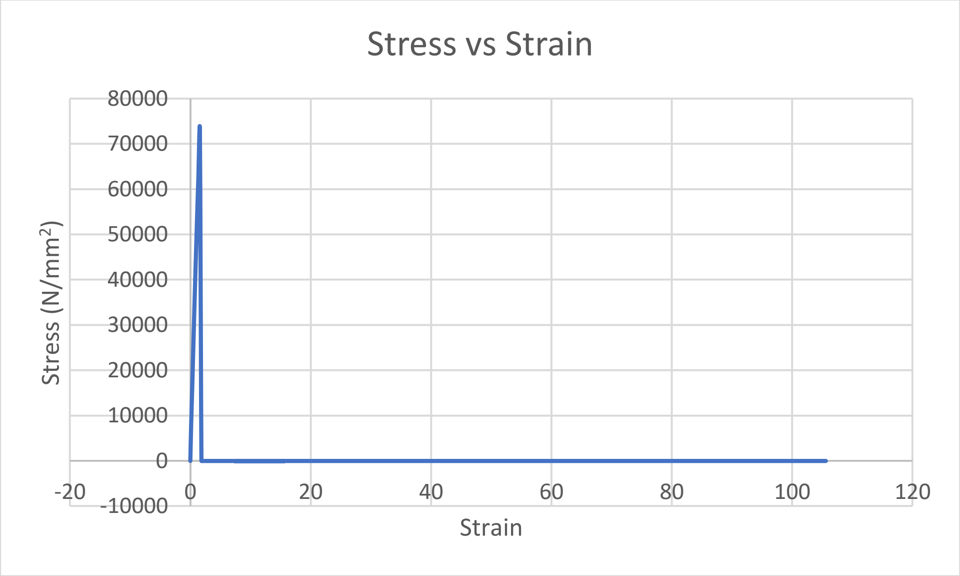

Figure B.5 (b) Element 21621; projectile velocity 520 m/s

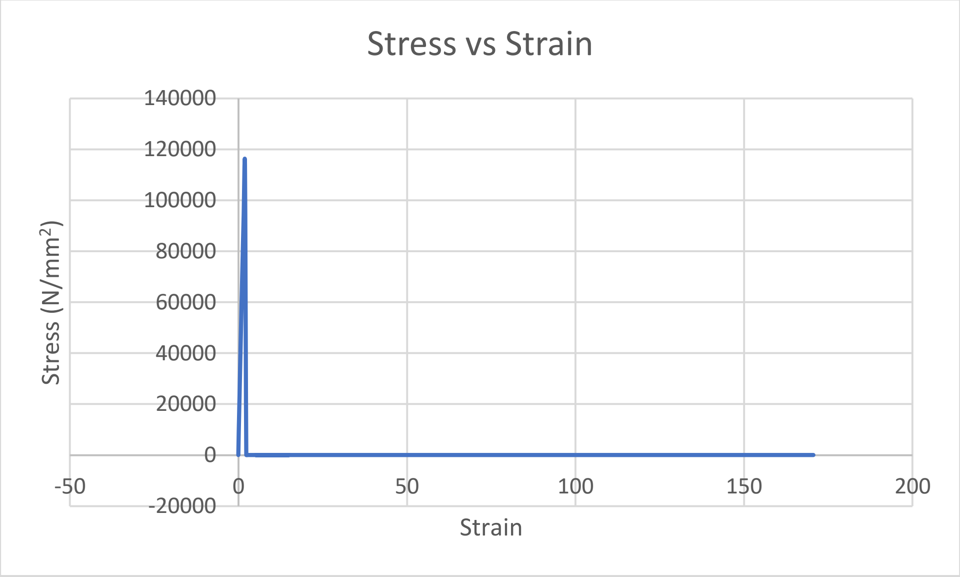

Figure B.5 (c) Element 21621; projectile velocity 800 m/s

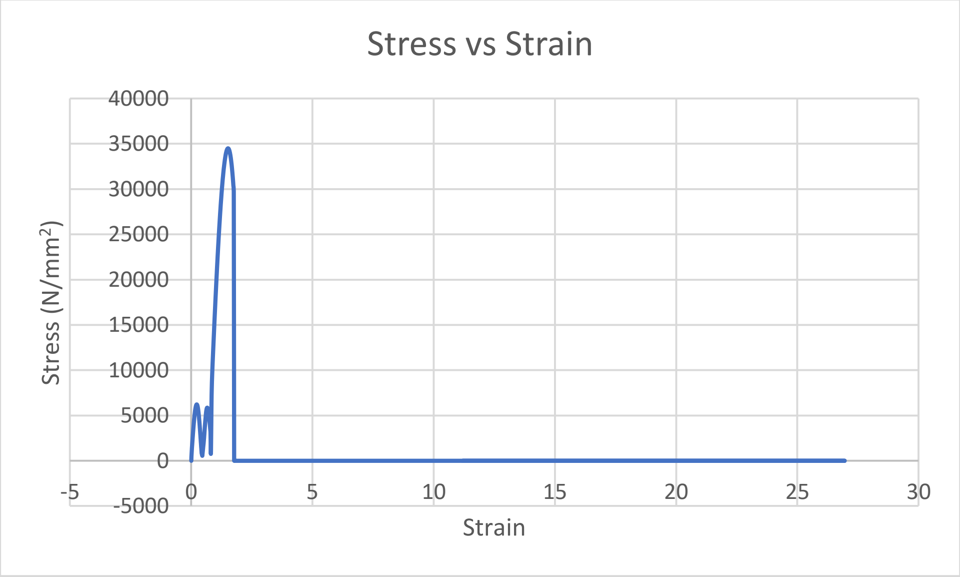

Figure B.6 (a) Element 21639; projectile velocity 100 m/s

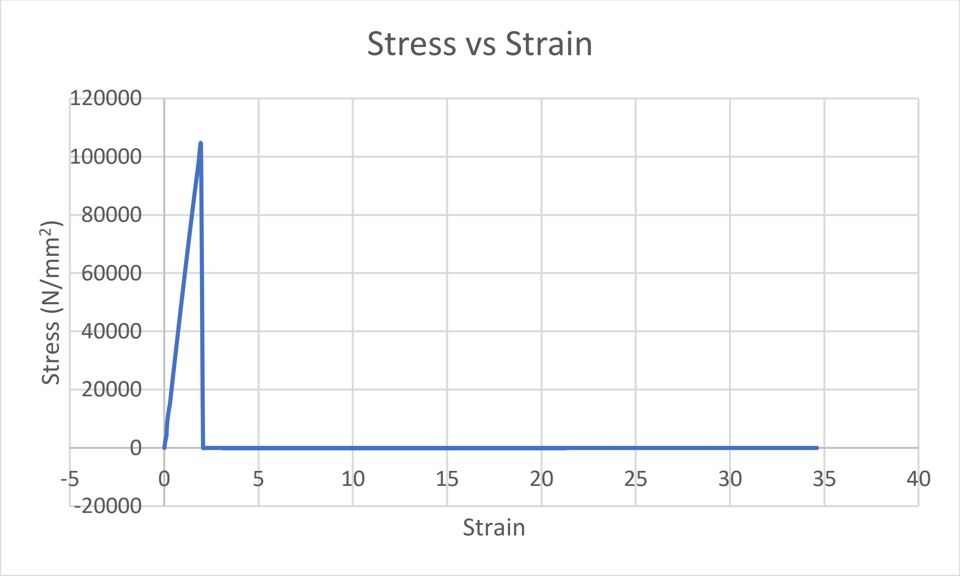

Figure B.6 (b) Element 21639; projectile velocity 520 m/s

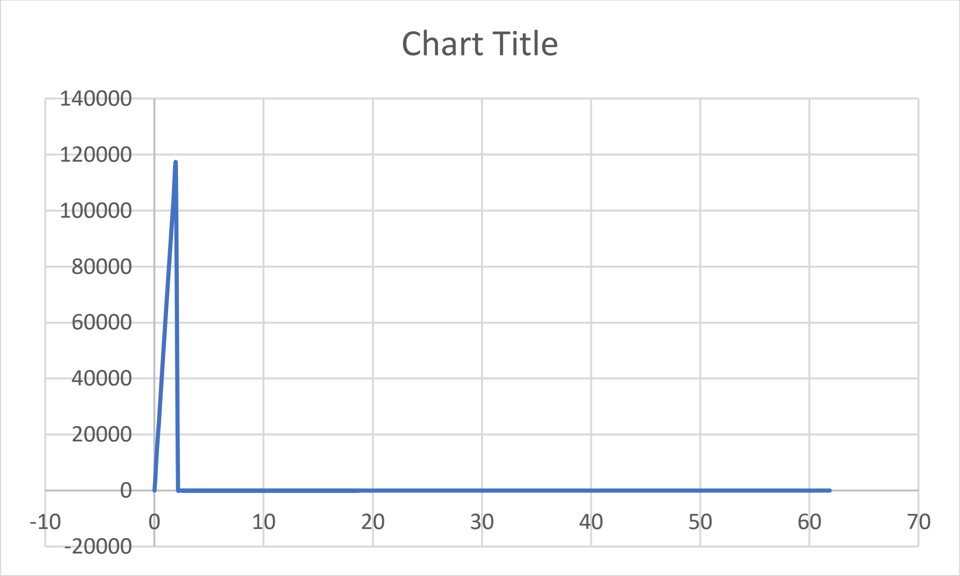

Figure B.6 (c) Element 21639; projectile velocity 800 m/s

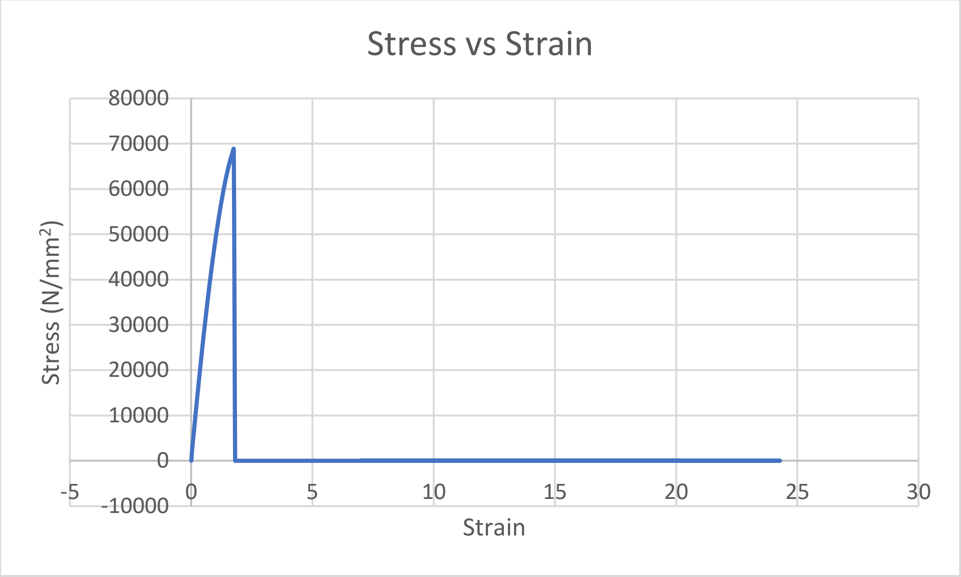

Figure B.7 (a) Element 22540; projectile velocity 100 m/s

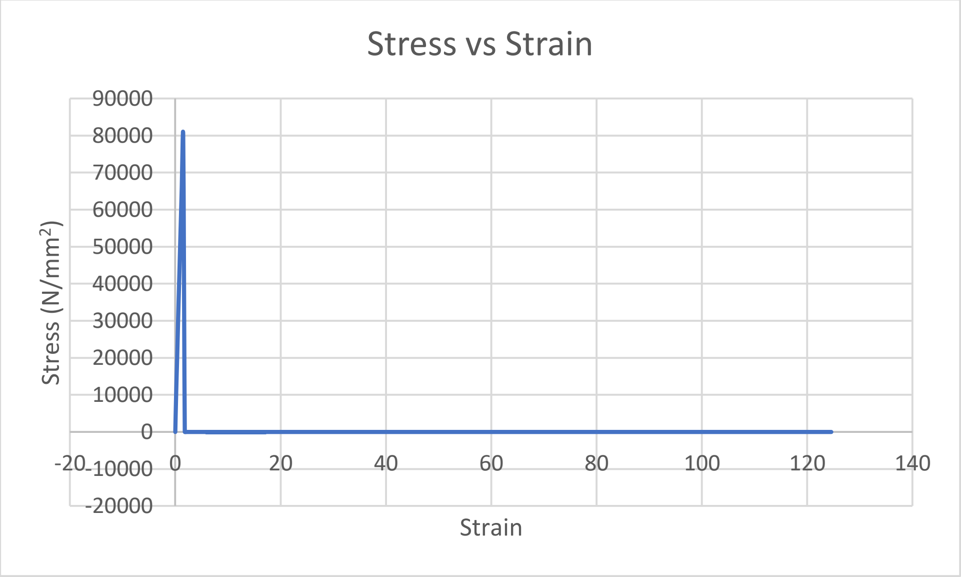

Figure B.7 (b) Element 22540; projectile velocity 520 m/s

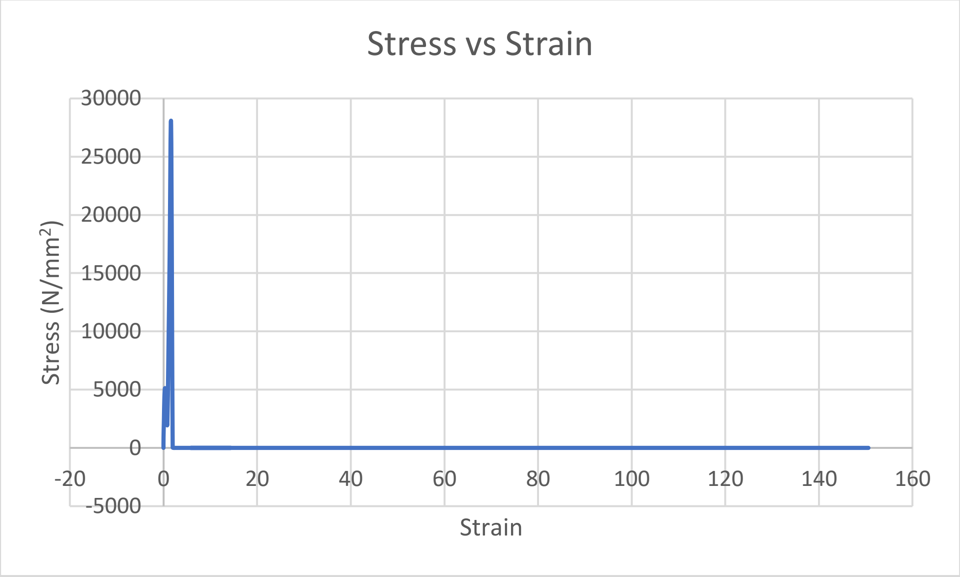

Figure B.7 (c) Element 22540; projectile velocity 800 m/s

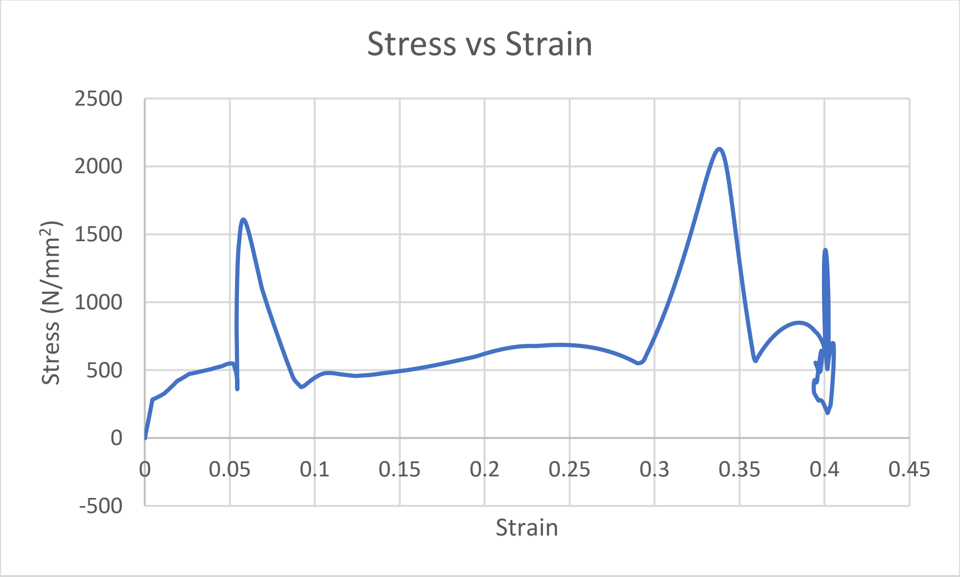

Figure B.8 (a) Element 22600; projectile velocity 100 m/s

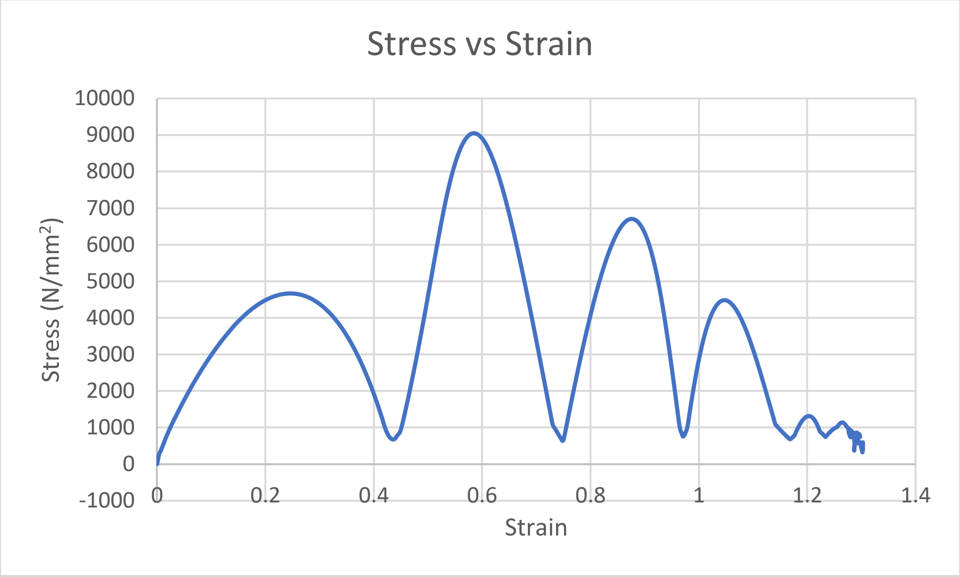

Figure B.8 (b) Element 22600; projectile velocity 520 m/s

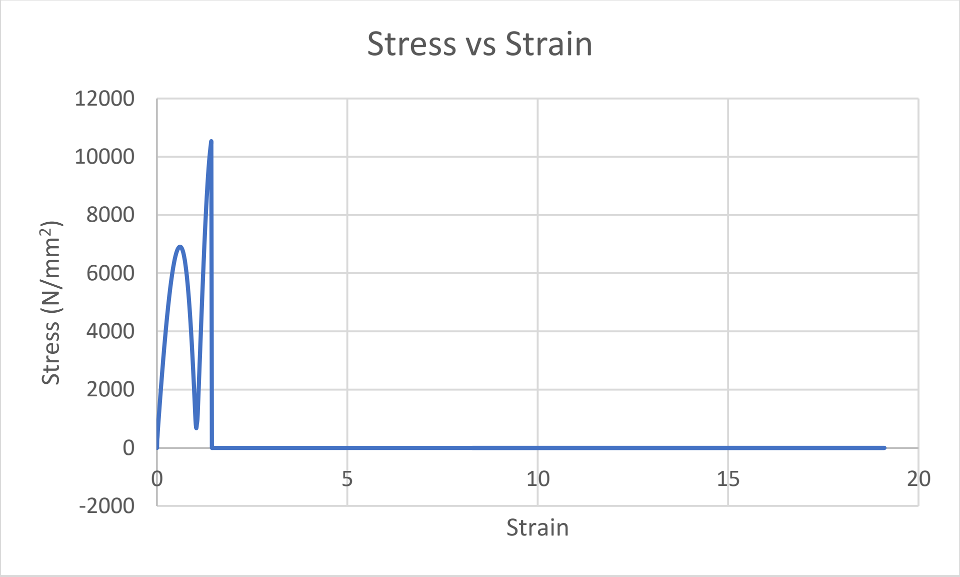

Figure B.8 (c) Element 22600; projectile velocity 800 m/s

REFERENCES

Abaqus/Explicit User's Manual (Version 6.14). Hibbitt, Karlsson & Sorensen, Inc.

Abdel-Wahed, M., et al. (2010). "Penetration of a small caliber projectile into single and multi-layered targets." *EPJ Web of Conferences, EDP Sciences*.

Abdulhamid, M. F. and C. Basaran (2001). "Influence of thermomigration on lead-free solder joint mechanical properties." *Journal of Electronic Packaging* 131 (1), 011002.

Abed, F. H. and G. Z. Voyiadjis (2005). "Plastic deformation modeling of AL-6XN stainless steel at low and high strain rates and temperatures using a combination of bcc and fcc mechanisms of metals." *International Journal of Plasticity* 21(8): 1618-1639.

Anderson Jr, C. E. and S. R. Bodner (1988). "Ballistic impact: the status of analytical and numerical modeling." *International Journal of Impact Engineering* 7(1): 9-35.

Arias, A., et al. (2008). "Numerical simulations of impact behaviour of thin steel plates subjected to cylindrical, conical and hemispherical non-deformable projectiles." *Engineering Fracture Mechanics* 75(6): 1635-1656.

Backman, M. E. and W. Goldsmith (1978). "The mechanics of penetration of projectiles into targets." *International Journal of Engineering Science* 16(1): 1-99.

Banerjee, A., et al. (2017). "Numerical simulation of ballistic impact of armour steel plate by typical armour piercing projectile." *Procedia Engineering* 173: 347-354.

Basaran, C. and E. Gunel (2015). "Damage Mechanics Unified Constitutive Modeling for Polymers." *Handbook of Damage Mechanics*, Springer: 681-720.

Basaran, C., et al. (2008). "Thermomigration induced degradation in solder alloys." *Journal of Applied Physics* 103 (12), 123520.

Basaran C. and S. Nie (2007). "A thermodynamics based damage mechanics model for particulate composites." *International Journal of Solids and Structures* 44 (3-4), 1099-1114.

Basaran, C., et al. (2003). "A thermodynamic model for electrical current induced damage." *International Journal of Solids and Structures* 40(26): 7315-7327.

Basaran, C. and S. Nie (2004). "An irreversible thermodynamics theory for damage mechanics of solids." *International Journal of Damage Mechanics* 13(3): 205-223.

Basaran, C. and H. Tang (2002). "Implementation of a thermodynamic framework for damage mechanics of solder interconnects in microelectronics packaging." *International Journal of Damage Mechanics* 11(1): 87-108.

Basaran, C. and R. Chandaroy (2000). "Using finite element analysis for simulation of reliability tests on solder joints in microelectronic packaging." *Computers & Structures* 74 (2), 215-231.

Basaran, C. and C.-Y. Yan (1998). "A thermodynamic framework for damage mechanics of solder joints." *Journal of Electronic Packaging* 120(4): 379-384.

Ben-Dor, G., et al. (2005). "Ballistic impact: recent advances in analytical modeling of plate penetration dynamics–a review." *Applied Mechanics Reviews* 58(6): 355-371.

Boltzmann, L. (1964). *Lectures on Gas Theory*, Univ of California Press.

Børvik, T., et al. (2002). "Perforation of 12 mm thick steel plates by 20 mm diameter projectiles with flat, hemispherical and conical noses: Part I: Experimental study." *International Journal of Impact Engineering* 27(1): 19-35.

Corbett, G., et al. (1996). "Impact loading of plates and shells by free-flying projectiles: a review." *International Journal of Impact Engineering* 18(2): 141-230.

Corran, R., et al. (1983). "Impact loading of plates—an experimental investigation." *International Journal of Impact Engineering* 1(1): 3-22.

Dey, S., et al. (2007). "On the ballistic resistance of double-layered steel plates: an experimental and numerical investigation." *International Journal of Solids and Structures* 44(20): 6701-6723.

Fernandez Ambrosini, J. (2014). *Simulation of ballistic impacts in steel plates*, Universitat Politècnica de Catalunya.

Golsdmith, W. and S. Finnegan (1971). "Penetration and perforation processes in metal targets at and above ballistic velocities." *International Journal of Mechanical Sciences* 13(10): 843-866.

Gomez, J. and C. Basaran (2006). "Nano indentation of Pb/Sn solder alloys; experimental and finite element simulation results." *International Journal of Solids and Structures* 43 (6), 1505-1527.

Gomez, J. and C. Basaran (2005). "A thermodynamics based damage mechanics constitutive model for low cycle fatigue analysis of microelectronics solder joints incorporating size effects." *International Journal of Solids and Structures* 42(13): 3744-3772.

Gupta, N. and V. Madhu (1997). "An experimental study of normal and oblique impact of hard-core projectile on single and layered plates." *International Journal of Impact Engineering* 19(5-6): 395-414.

Hibbitt, et al. (2001). *ABAQUS/Explicit: user's manual*, Hibbitt, Karlsson and Sorenson Incorporated.

Jankowiak, T., et al. (2014). "Ballistic behavior of steel sheet subjected to impact and perforation."

Jena, P. K. and P. Senthil (2016). "Effect of tempering time on the ballistic performance of a high strength armour steel." *Journal of applied research and technology* 14(1): 47-53.

Johnson, G. and W. Cook (1983). "A constitutive model and data for metals subjected to large strains, strain rates, and high pressures." *Proceedings of the 7th International Symposium On Ballistics.*

Kumar, M., et al. (2017). "Simulation and Analysis of Ballistic Impact Using Continuum Damage Mechanics (CDM) Model." *Procedia Engineering* 173: 190-197.

Lemaitre, J. (1984). "How to use damage mechanics." *Nuclear engineering and design* 80(2): 233-245.

Li, S. and C. Basaran (2009). "A computational damage mechanics model for thermomigration." *Mechanics of Materials* 41(3): 271-278.

Milke, J., et al. (2002). "A overview of fire protection in buildings." *Federal Emergency Management Agency, USA.*

Park, M., et al. (2005). "An optimization of a multi-layered plate under ballistic impact." *International Journal of Solids and Structures* 42(1): 123-137.

Rahman, N. A., et al. (2016). "Ballistic limit of high-strength steel and Al7075-T6 multi-layered plates under 7.62-mm armour piercing projectile impact." *Latin American Journal of Solids and Structures* 13(9): 1658-1676.

Recht, R. and T. Ipson (1963). "Ballistic perforation dynamics." *Journal of Applied Mechanics* 30(3): 384-390.

Rusinek, A., et al. (2009). "Experimental and numerical study on the perforation process of mild steel sheets subjected to perpendicular impact by hemispherical projectiles." *International Journal of Impact Engineering* 36(4): 565-587.

Rusinek, A., et al. (2007). "Constitutive relations in 3-D for a wide range of strain rates and temperatures–application to mild steels." *International Journal of Solids and Structures* 44(17): 5611-5634.

Sosnovskiy, L. A. and S. S. Sherbakov (2016). "Mechanothermodynamic entropy and analysis of damage state of complex systems." *Entropy* 18(7): 268.

Standard, B. (2006). "Eurocode 3—Design of steel structures—." *BS EN 1993-1* **1**: 2005.

Tang, H. and C. Basaran (2001). "Influence of microstructure coarsening on thermomechanical fatigue behavior of Pb/Sn eutectic solder joints." *International Journal of Damage Mechanics* 10 (3), 235-255

Temfack, T. and C. Basaran (2015). "Experimental verification of thermodynamic fatigue life prediction model using entropy as damage metric." *Materials Science and Technology* 31(13): 1627-1632.

Tupek, M., et al. (2013). "An approach for incorporating classical continuum damage models in state-based peridynamics." *Computer methods in applied mechanics and engineering* 263: 20-26.

Yao, W. and C. Basaran (2013). "Computational damage mechanics of electromigration and thermomigration." *Journal of Applied Physics* 114(10): 103708.

Yao, W. and C, Basaran (2012). "Electromigration analysis of solder joints under AC load: A mean time to failure model." *Journal of Applied Physics* 111 (6), 063703, 30.

Zerilli, F. J. and R. W. Armstrong (1987). "Dislocation-mechanics-based constitutive relations for material dynamics calculations." *Journal of Applied Physics* 61(5): 1816-1825.

Zhao, Y., et al. (1999). "Thermomechanical behavior of micron scale solder joints: An experimental observation." *Journal of the Mechanical Behavior of Materials* 10 (3), 135-146, 1999

Zukas, J. A., et al. (1982). "Penetration and perforation of solids." *Impact dynamics*: 155-214.